# Female *versus* male biological identities of nanoparticles determine the interaction with immune cells in fish

Yuya Hayashi,*[abc] Teodora Miclaus,[cd] Sivakumar Murugadoss,[b] Masanari Takamiya,[b] Carsten Scavenius,[a] Kasper Kjaer-Sorensen,[a] Jan J. Enghild,[a] Uwe Strähle,[b] Claus Oxvig,[a] Carsten Weiss[b] and Duncan S. Sutherland*[c]

[a.] *Department of Molecular Biology and Genetics, Aarhus University, Gustav Wieds Vej 10, 8000 Aarhus C, Denmark. E-mail: yuya.hayashi@mbg.au.dk*

[b.] *Institute of Toxicology and Genetics, Karlsruhe Institute of Technology (KIT), Hermann-von-Helmholtz-Platz 1, 76344 Eggenstein-Leopoldshafen, Germany.*

[c.] *iNANO Interdisciplinary Nanoscience Center, Aarhus University, Gustav Wieds Vej 14, 8000 Aarhus C, Denmark. E-mail: duncan@inano.au.dk*

[d.] *Nano4Environment Unit, Department of Life Science, INL International Iberian Nanotechnology Laboratory, Avenida Mestre Jose Veiga s/n, 4715-330 Braga, Portugal.*

† Electronic supplementary information (ESI) available: Supplemental descriptions of experimental methods, figures and tables.

**Environmental significance**

Nanoparticles infiltrating an organism's biological compartments experience spontaneous macromolecular adsorption forming a corona of biomolecules. This concept has proved of particular relevance to nanomedicine/toxicology in linking nanoparticles' interfacial properties and biological responses. Surprisingly little is known, however, about how biomolecular coronas take shape and behave within non-mammalian organisms, the vital components of environmental health. What we have found is that the biomolecular coronas can be formed in a sex-specific manner and determine the nanoparticle-cell interactions in fish. Our findings suggest that sex of the fish is a critical factor for extrapolation of the *in vitro* studies, and in general that ecological risk assessments of nanomaterials may require careful consideration for the unique repertoire of proteins in a given biological system.

**Abstract**

Biomolecule decoration of nanoparticles provides a corona that modulates how the nanoparticles interact with biological milieus. The corona composition has proved to reflect the differences in the repertoire of proteins to which the nanoparticles are exposed, and as a result the same nanoparticles can acquire a differential biological identity. Here we examined whether a unique biological identity acquired from sex-specific protein repertoires could alter the degree of nanoparticle uptake by cognate immune cells. We chose zebrafish as a model species of which blood plasma is sexually contrasted by the unique presence/absence of the egg yolk precursor protein vitellogenin. Sex-specific protein coronas were thus formed around 70 nm $SiO_2$ nanoparticles using female/male blood plasma from zebrafish or fetal bovine serum as a non-native reference. In contrast to protein coronas formed of male blood plasma, a "female" biological identity of the nanoparticles was represented by prevailing contribution of vitellogenins to the corona proteome. We then exposed zebrafish blood cells to the three types of pre-formed nanoparticle-protein complexes and compared nanoparticle uptake using flow cytometry. Lymphoid and myeloid populations of the blood cells preferentially accumulated the nanoparticles with a female biological identity, irrespective of the sex of the fish from which the cells were obtained. The concept of repertoire differences in the corona proteome therefore deserves further attention, as various factors such as sex-specific biological conditions exemplified in this study could alter the nanoparticle-cell interactions.

## Introduction

Nanoparticles encounter a dazzling variety of chemical and macromolecular entities once they are released into the environment (reviewed in ref 1). The physical interaction of nanoparticles with macromolecules of biological origin, in particular, creates a biomolecular corona – an extensively studied concept in the biomaterials field.[2] Only recently, this concept has attracted attention as a factor in the evaluation of potential ecological risks associated with nanoparticle exposure of non-mammalian organisms.[3-6] Proteins, among other biomolecules, represent the major component that determines how nanoparticles behave rather differently depending on the corona characteristics (see refs 2, 7, 8 for a comprehensive review). We have previously reported a proof of concept that the biomolecular corona can provide a species-specific identity of nanoparticles recognised as "native" or "exotic" in earthworms,[6] subsequently supported by Canesi and colleagues using marine bivalves as a model organism.[4] This suggests that the same nanoparticles can acquire a quite different biological identity, depending on the repertoire of proteins to which they are exposed.

Here we propose that differences in the protein repertoire within the same species has the potential to give systematic alterations of the biomolecular corona, and sex may be a biological parameter that contributes to such differences. For example, proteomic profiling of human blood plasma indicated a higher abundance of oestrogen-related proteins in female than in male.[9] This sex difference, including certain sex-specific physiological conditions (e.g. pregnancy), would potentially lead to differential formation of protein coronas.[10] Conceptually, the differences in the protein repertoire reflect the unique absence, presence or modification of certain proteins. Should such proteins entail a high affinity for nanoparticle surfaces, formation of a unique protein corona would result. In our previous study, for example, it was the unique presence of species-

specific endogenous proteins in the corona that seemed to have primed immune recognition and uptake of the nanoparticles.[6] Likewise in this study the sex-specific presence/absence of endogenous proteins in the repertoire could potentially give rise to a sex-specific biological identity and associated immune recognition of the nanoparticles.

Blood plasma contains a broad array of functional proteins, many of which are central to immunity, e.g. immunoglobulins and complement factors. This repertoire of blood proteins is intrinsically native to leukocytes. For instance, peripheral blood lymphocytes are trained/regulated to tolerate endogenous biomolecules ("self" exclusion) while myeloid phagocytes make use of opsonic plasma markers bound to foreign materials and pattern recognition receptors for "non-self" detection. It is therefore of particular interest to ask how the two arms of self/non-self discrimination programs, operated by lymphoid and myeloid cell lineages respectively, handle nanoparticles with a non-native or sex-specific biological identity. To address this biological question, we chose zebrafish as a model species that allows both sexing by morphological characteristics and harvesting of blood plasma and primary leukocytes. Another key advantage of using zebrafish is that the blood plasma composition is naturally altered by a sex-specific biological trait; adult female zebrafish maintain a high level of specific precursor proteins in the blood for the production of egg yolk during vitellogenesis. This allows a clear comparison of the protein repertoire with and without sex-specific proteins and thereby unique biological identities.

For the first time we show here that a sex selective formation of the protein corona translates into nanoparticles' sex-specific biological identity in fish, and that the blood cells interact differentially with those nanoparticles *in vitro*. We discuss the observed differences in the corona profiles and respective changes in the degree of nanoparticle accumulation, referring

to compositional uniqueness of the nanoparticles' biomolecular corona and cell-type dependency of self/non-self recognition. Our findings shed light on the poorly-understood behaviour of blood cells towards diverse identities of nanoparticles that would play a vital role in the fields of nanomaterials ecotoxicology, bionanoscience and human toxicology.

## Materials and Methods

### Collection of zebrafish blood plasma.

**Zebrafish.** Zebrafish (*Danio rerio*, wild-type strains) were bred and maintained in accordance with the German law under animal welfare regulations (Regierungspräsidium Karlsruhe, Germany, Az. 35-9185.64/BH KIT). Euthanasia of fish for scientific purposes was performed as per the German legislations (TSchG (18/05/2006 and 13/07/2013) and TierSchVersV (01/08/2013)). Several wild-type strains including AB, $AB_2O_2$ and AB/WIK were used for blood collection, while the AB/WIK strain was exclusively used for harvesting of whole kidney marrow (WKM) cells. The age of adult fish scheduled for sacrifice ranged from 1-2 years. Neither strain nor age critically affected the consistent patterns of major plasma protein composition.

**Blood collection.** To obtain a large volume of blood from each fish, a centrifuge-based method reported by Babaei and colleagues[11] was employed with modifications to accommodate large-sized fish (see ESI† for details). Briefly, fish were first anesthetised with 0.02% tricaine (3-amino benzoic acid ethyl ester) and euthanised in ice-water. Each euthanised fish had its tail amputated, and blood was collected from the wound along with anticoagulation buffer prepared of PBS containing 10 mM EDTA (BioUltra, Sigma-Aldrich) and a mixture of 100 U/mL penicillin and 100 $\mu$g/mL streptomycin (Gibco). The blood was transferred to a Protein LoBind tube (Eppendorf) and spun at 13800*g* for 15 min at 8°C. If haemolysis was apparent, the tube was discarded. The clear supernatant (plasma) was pooled and stored at -80°C until use (within a month). Normally 6 female or male fish were sacrificed in one session and each batch of pooled plasma had a typical protein yield of 100-200 $\mu$g per fish. The obtained blood plasma is hereafter

referred to as DrBP-F or DrBP-M (*D. rerio* blood plasma - female or male, respectively). DrBP (Mix) is a 1:1 mixture of the two.

**$SiO_2$ nanoparticle-protein complexes.**

**Nanoparticles**. The fluorescent silica particles sicastar-greenF (plain surface, nonporous, 70 nm in diameter, fluorescein isothiocyanate-labelled; ex/em = 485/510 nm) was purchased from micromod Partikeltechnologie GmbH (Germany) and used throughout the experiments. Dissociation of the dye (fluorescein isothiocyanate; FITC) from the silica matrix was tested in PBS using Amicon Ultra centrifugal filter units (3 kDa cut-off regenerated cellulose membrane, Merck Millipore). The particle-free filtrate showed negligible fluorescence (~3% of the total fluorescence before filtering) measured at ex/em = 485/508 nm on a Biotek Lambda Fluoro 320 Microplate Fluorescence Reader (MWG-Biotech, Ebersberg, Germany).

**Incubation of nanoparticles.** The protein concentrations of the DrBP series (DrBP-F, DrBP-M, DrBP-Mix) and fetal bovine serum (FBS; Sigma) were adjusted to 1 mg/ml and 2 mg/ml, respectively, using the anticoagulant buffer. These protein concentrations correspond to approximately 2.5-5.0% of the original protein concentrations in whole blood/serum. These concentrations were chosen partly because of the limitation of the adult fish availability for blood collection but also in accordance with the concentration range of proteins used in cell culture systems. The protein solutions were centrifuged at 16000*g* for 3 min at room temperature (RT) to remove any insoluble protein aggregates, and the supernatants were then incubated with the $SiO_2$ nanoparticles (200 $\mu$g/ml) at 26°C for 24 h in darkness. To minimize non-specific binding of proteins to the tube wall, Protein Lobind tubes were used in all steps of incubation and centrifugal isolation of nanoparticle-protein complexes. At the chosen ratio of nanoparticles-to-proteins, theoretically, there is a 22 (the DrBP series) or 44 (FBS) times excess of proteins,

enough to cover the nanoparticle surface. The nanoparticle-protein complexes were isolated from unbound and loosely-bound proteins by a well-established centrifugation technique as described previously.[6] Nanoparticle-free blanks were separately prepared and we confirmed by SDS-PAGE that no protein aggregates were unintentionally spun down during the centrifugal isolation steps. Details of the incubation conditions and the centrifugal isolation method are described in ESI†.

**Protein corona profiling and characterisation.**

**Protein corona profiling.** SDS-PAGE and tandem mass spectrometry were performed as described previously[6] and technical details can be found in ESI†. The gel images were analysed using the plot profile tool in Fiji/ImageJ[12, 13] to quantify the staining intensity and run length. The whole process starting from the formation of the nanoparticle-protein complexes to documentation of the stained gels was repeated three times to ensure reproducibility.

**Characterisation.** The physico-chemical properties of each type of $SiO_2$ nanoparticle-protein complex were characterised in a similar manner as previously described.[6] Briefly, transmission electron microscopy (TEM), nanoparticle tracking analysis (NTA), dynamic light scattering (DLS) and zeta potential analysis were performed and the details are described in ESI†.

**Cellular uptake of the nanoparticle-protein complexes.**

**Whole kidney marrow (WKM) cells.** Wild-type adult zebrafish were first anesthetised with 0.02% tricaine and euthanised in ice-water. WKM is the haematopoietic organ in adult zebrafish[14] and was excised as described[15] to harvest all types of cells belonging to the haematopoietic lineage. Briefly, WKM was placed in cCCM (the components of which are described below) on ice, triturated by gentle pipetting, and passed through a 35-$\mu$m nylon mesh cell strainer (BD Falcon). The WKM cells were spun down at 230*g* for 5 min, resuspended and filtered again. The cells were centrifuged again and resuspended in cCCM. The cCCM consisted

of RPMI-1640 medium with L-glutamine, phenol red and 25 mM HEPES (Gibco), supplemented with a mixture of 100 U/mL penicillin and 100 $\mu$g/mL streptomycin (Gibco) and 5% FBS (Sigma).

**Cell sorting and staining.** For optimal cell sorting, the WKM cells were resuspended in sort buffer (PBS containing 0.1% bovine serum albumin, 10 mM HEPES and a mixture of 100 U/mL penicillin and 100 $\mu$g/mL streptomycin, sterile-filtered). Light scatter-based sorting of the WKM cells was performed on a FACS Aria II flow cytometer (BD Biosciences), followed by post-sort analysis of the two sorted groups, lymphoid and myeloid populations. The sorted cells were spun down at 900 rpm for 3 min onto pre-wetted glass slides using a Cytospin 4 Cytocentrifuge (ThermoScientific) and air-dried overnight. The cells were then stained by May-Grünwald (8 min; Sigma) and Giemsa (1:5 dilution, 5 min; Carl Roth GmbH & Co., Germany) solutions before mounting in EUKITT (Sigma-Aldrich) for optical microscopy (DM5000B, Leica Microsystems).

**Exposure.** Three types of the $SiO_2$ nanoparticle-protein complexes (with a pre-formed corona of DrBP-F, DrBP-M or FBS) were prepared as described above except that the complexes were centrifuged for a prolonged duration (40 min) followed by redispersion in MilliQ water without further washing steps. With this centrifugation parameter, typically 86 ± 6% (mean ± S.D., $n = 4$, based on fluorescence measurements) is recovered after redispersion without severely compromising the colloidal stability. WKM cells collected from either female or male fish were exposed for 2 h to each type of nanoparticle-protein complexes (nominal concentrations: 6.125, 12.5, 25 and 50 $\mu$g/ml) or a control (MilliQ water) in cCCM at the density of $5\times10^5$ cells/ml at 28°C in darkness. *Escherichia coli* BioParticle (FITC-conjugated, non-opsonised, 10 bacteria per cell; Molecular Probes) was included as a positive control for uptake/binding.

**Flow cytometry.** Following exposure, the cells were harvested using Accutase (Gibco), spun down at 370*g* for 5 min, washed once and resuspended in PBS containing 1 $\mu$g/mL 7-aminoactinomycin D (Molecular Probes). The samples were kept on ice until analysis by flow cytometry (FACScan, BD Biosciences). The 488 nm laser was used for excitation; FITC fluorescence and the dead cell stain 7-aminoactinomycin D were detected in FL1 (530/30 BP filter) and FL3 (670 LP filter), respectively. Bleeding of FITC fluorescence into the FL3 channel was compensated using an unstained/FITC-positive control (*E. coli* BioParticles). For each sample, a total of >45000 cells were gated for analysis in FlowJo ver 7.6.5 (FlowJo LLC, OR). Among those, lymphoid and myeloid populations were analysed separately based on their characteristic light scatter profiles as verified by the preceding sorting/staining study. The two populations had a negligible fraction of dead cells (<5%) in all samples. With this gating strategy, other recorded events (majority of erythrocytes, precursor cells, cell debris and, if present, agglomerates of nanoparticles) were thus excluded from analysis. Three independent assays on WKM cells collected from each sex (female and male) were performed using different batches of DrBP-F and -M. The differences in the mean FITC fluorescence intensity between the cells exposed to the three types of nanoparticle-protein complexes at each test concentration were statistically tested in R using Levene's Test for equality of variance and one-way analysis of variance (ANOVA) with a post hoc multiple means comparison (Tukey's HSD). Prior to all the parametric tests, measurement values were log-transformed to satisfy the assumption of normal distribution and significance was determined as $\alpha = 0.05$.

**Confocal laser scanning microscopy (CLSM).** The WKM cells were exposed likewise to the three types of the nanoparticle-protein complexes (nominal 50 $\mu$g/ml) or the positive control (*E. coli* BioParticles, 10 per cell), washed in PBS, and fixed for 20 min at RT in 10% neutral-

buffered formalin (Sigma). The fixed cells were PBS-washed and stained by wheat germ agglutinin (WGA) conjugated with Alexa633 (5 $\mu$g/ml; Molecular Probes) and DAPI (300 nM; Molecular Probes) for 20 min at RT. After PBS washing, the stained cells were resuspended in sort buffer for light scatter-based cell sorting as described above. The sorted cells were cytospun onto glass slides and mounted with SlowFade Diamond Antifade Mountant (Molecular Probes). Imaging was performed on a Leica TCS SP5 upright confocal microscope (Leica Microsystems) with lasers at 405 nm (DAPI), 488 nm (FITC) and 633 nm (WGA-Alexa633). Selected high magnification images were deconvolved using a Leica Application Suit X software with a 3D deconvolution module and post-processed with Fiji/ImageJ.[12, 13]

## Results and discussion

### Sex- and species-specificity of the protein repertoire in zebrafish blood plasma.

The repertoire of proteins that nanoparticles encounter determines the corona composition. We began first by screening sex differences in the repertoire of blood proteins in adult zebrafish (*Danio rerio*). Blood plasma was collected separately from females and males across several wild-type strains, and we verified by SDS-PAGE that the repertoire of blood proteins is primarily sex-specific in zebrafish. The obtained blood plasma was thus referred to as DrBP-F or DrBP-M (*D. rerio* blood plasma - female or male, respectively). DrBP (Mix) is a 1:1 mixture of the two. In general there is a characteristic bias towards certain proteins for female (DrBP-F: rich in 70-200 kDa proteins) and for male (DrBP-M: rich in 40-70 kDa proteins), apart from low-molecular weight proteins (below 40 kDa) that were commonly abundant (Fig. 1, right lanes: "NP –"). This is in good agreement with other studies where the sex-specific proteomes were catalogued based on zebrafish blood plasma.[11, 16] This differential repertoire according to sex is directly linked to the oviparous reproductive system in zebrafish, as female fish maintain a high plasma concentration of egg yolk precursor proteins, specifically the family of vitellogenins.[11, 16] Another factor to keep in mind is that, despite the deep evolutionary conservation of the plasma protein repertoire, DrBP lacks serum albumin, one of the most abundant blood proteins in higher vertebrates such as mammals.[16] Consequently, the key intra-species difference in the protein repertoire between DrBP-F (female) and DrBP-M (male) arises primarily from the production of vitellogenins, while the major differences from mammals are the presence of vitellogenins (in female) and the absence of serum albumin.

### Sex-specific biological identity of nanoparticles.

We then characterised nanoparticle-protein complexes formed with three protein sources: DrBP-

F, DrBP-M and FBS (fetal bovine serum, unspecified sex) as a reference for mammalian serum proteins. We incubated 70 nm $SiO_2$ nanoparticles labelled with FITC separately in the three types of protein source for 24 h at the physiological temperature (26°C for zebrafish), thereby allowing spontaneous formation of respective protein coronas around the nanoparticles.[17] The nanoparticle-protein complexes thus formed were isolated by a well-established centrifugation technique[8] and the bound proteins were separated by SDS-PAGE, as described previously.[6]

The sex differences in the repertoire translated into a differential protein corona pattern of strongly bound proteins distinct for female and male, whereas low-molecular weight proteins were commonly found in both sexes (Fig. 1; see Tables S1† & S2† for the list of protein IDs). Although precise quantitation was not performed in the present study, the total mass of the corona proteins was in a comparable range between DrBP-F and -M, while less protein was recovered from FBS. The total protein mass available for $SiO_2$ nanoparticles during incubation was 500 $\mu$g (DrBP) or 1000 $\mu$g (FBS), about <1-2% of which was strongly bound to 100 $\mu$g of the nanoparticles (theoretically, $3\times10^{11}$ particles with a total outer surface area of 43 $cm^2$). As predicted for human plasma,[18] a large excess of zebrafish plasma proteins is likely required for the colloidally stable formation of the protein corona. Among the strongly bound proteins in the corona, the female-specific proteins were identified to be several variants of vitellogenin, one of the most abundant protein families in DrBP-F. Each isoform was identified in most of the analysed bands including those at low molecular weights; they are likely cleaved chains of vitellogenins. Full-length vitellogenin has a theoretical molecular mass of around 148 kDa, while, for example, its two major cleavage products are 114 kDa (lipovitellin heavy chain, LvH) and 26 kDa (lipovitellin light chain, LvL).[19] This is supported by the sequence coverage maps of peptides analysed by tandem mass spectrometry (Fig. S2†). The lack of vitellogenin in the male

counterpart seemed to have resulted in preferential enrichment of fetuin, a transporter glycoprotein commonly found in blood plasma especially during fetal life.[20] The corona proteins found substantially in both sexes were apolipoprotein A-I and haemoglobin subunit β, both of which were also relatively abundant in the respective blood plasma (Fig. 1, right lanes: "NP −"). Consequently, the protein coronas formed of DrBP-F and of DrBP-M appear similar except for the dominant contribution of vitellogenin leaving little room for fetuin. When the female and male blood plasma was mixed 1:1 ("DrBP (Mix)"), the corona composition mimicked the calculated average of that in DrBP-F/M except that vitellogenin was slightly more enriched than predicted (Fig. 1, the peaks in question denoted with an asterisk). The implication is that it is the surface accessibility that may limit the local accumulation of vitellogenin rather than binding kinetics (i.e. concentration-limited). The latter seems to apply for other proteins; for example, when the peak heights were compared between the corona proteins ("NP +") and the respective total proteins ("NP −"), we noticed that the peak representing apolipoprotein A-I in the coronas formed of DrBP-F/M was consistently lower than that in the respective total proteins (DrBP-F, 85 ± 8%; DrBP-M, 84 ± 8%; mean ± S.D., $n = 3$).

Based on the obtained protein IDs (Tables S1† & S2†), we also sought to discover protein properties such as overall hydropathy (as GRAVY score) and electrostatic charges (inferred from p*I*) that may play a role in the protein corona formation. This approach failed to provide a conclusive picture, as is often the case even with a quantitative proteomic approach.[21, 22] Notably, however, vitellogenin is endowed with a conserved lipid transport domain; this suggests universal tendency of lipid-binding proteins (e.g. apolipoprotein) having a high affinity for $SiO_2$ surfaces. Indeed, the proteins identified in the long-lived corona formed of FBS were dominated by strong enrichment of apolipoprotein A-I despite the abundance of albumin, a

protein commonly found in nanoparticle-protein coronas. Apolipoprotein A-I is frequently reported as an essential contributor to hardening of the plasma/serum protein corona around $SiO_2$ nanoparticles,[18, 21, 22] and also to a lesser extent other types of nanoparticles such as those made of polystyrene,[18, 23] gold,[24, 25] silver[25] and iron oxide[26] as well as soft nanoparticles such as copolymer formulations[27] (reviewed in ref 28). In fact, fish apolipoprotein A-I was identified to be the dominant protein in the corona around 200 nm polystyrene particles following 1 h incubation in a range of fish sera.[29] Given that apolipoprotein A-I is a common protein between DrBP and FBS, its identification in all three types of tested hard coronas seems plausible. On the contrary, the presence or absence of vitellogenin and serum albumin in the protein repertoire determined the sex- and species-specificity of the nanoparticles' biological identity, respectively.

**Characterisation of $SiO_2$ nanoparticle-protein complexes.**

Interaction of nanoparticles and proteins impacts the physico-chemical behaviour of the assembled complexes. This presents a potential confounding factor for testing of the nanoparticles' differential biological identity on cellular recognition and uptake. Here we confirmed a typical core-shell structure of the complexes in the dry state and limited multimeric assemblies of the complexes in solution (Fig. 2). Considering the narrow distribution of the pristine $SiO_2$ nanoparticles, the peak shift from 75 nm to 100 nm could be attributed to the size increase by the hydrated protein layers (~12.5 nm increase in hydrodynamic radius). Shifts of comparable sizes are commonly observed both for $SiO_2$ and other types of nanoparticles.[6, 18, 21, 30] It should be noted that the observed increase in the hydrodynamic diameter does not directly correlate with the state of the corona characterised using centrifugal isolation approaches (e.g. TEM imaging and SDS-PAGE in this study). Unlike for DLS and NTA, the nanoparticle-protein complexes are extensively washed prior to analysis so that only the strongly-bound proteins are

retained in the corona. The in-solution characterisation techniques such as DLS and NTA therefore provide more relevant information on the effective size of coronas and the colloidal stability of the complexes. The broadening of the size distribution peak in DLS and appearance of multimodal peaks tailing towards larger sizes resolved in NTA are likely the indication of polydisperse clusters formed of two or more complexes. The complexes made with the DrBP series had similar mean hydrodynamic sizes while those made with FBS were slightly larger (Table 1).

Due to the limited availability of DrBP, we opted for using FBS as protein supplement to complete the cell culture media for the nanoparticle uptake assays. As previously,[6] we pre-formed the nanoparticle-protein complexes and characterised them in the presence of 5% FBS (complete cell culture media or cCCM) to underpin their stability and tolerance to retain the original biological identity. The former was achieved by DLS, since NTA can only characterise very low particle concentrations while DLS allows sizing at the same concentration of nanoparticles as in the *in vitro* assays. An increase in the hydrodynamic size and reduction of $\zeta$ potential were apparent in all cases, possibly through soft interactions with proteins supplemented (5% FBS) and/or formation of additional multimeric clustering upon centrifugation (Table 1; Fig. S4†). Nonetheless, even after secondary incubation in cCCM, the hard protein corona appeared to have retained its biological identity without considerably changing its major pattern of proteins (Fig. S5†). We believe therefore that the compositional uniqueness of each type of long-lived protein coronas, which also naturally determines the interfacial characteristics of the nanoparticle-protein complexes, represents the most influential variable for the recognition and uptake by cellular components of the immune system.

**Table 1.** Physico-chemical characterisation of $SiO_2$ nanoparticle-protein complexes.

| | | DLS | | | |
|---|---|---|---|---|---|
| | **NTA hydrodynamic diameter (nm)[a]** | **hydrodynamic diameter (nm)[b]** | | **ζ potential (mV)[c]** | |
| | | | **in cCCM** | | **+ cCCM** |
| reference (pristine) | 76.8 ± 18.1 | 73.6 ± 17.2 | n.a. | –42.7 ± 1.7 | n.a. |
| DrBP-F | 110.5 ± 39.5 | 112.0 ± 43.9 | 140.7 ± 51.4 | –31.6 ± 1.3 | –21.5 ± 0.8 |
| DrBP-M | 123.7 ± 37.0 | 103.7 ± 44.5 | 138.0 ± 63.0 | –32.4 ± 1.0 | –26.2 ± 0.7 |
| DrBP (Mix) | 112.1 ± 34.6 | 106.3 ± 43.2 | 136.3 ± 63.6 | –30.9 ± 0.6 | –22.1 ± 0.8 |
| FBS | 148.4 ± 51.1 | 129.7 ± 52.0 | 174.3 ± 84.7 | –31.3 ± 1.0 | –27.5 ± 0.5 |

Abbreviations: DrBP, *Danio rerio* blood plasma (F for female, M for male); NTA, nanoparticle tracking analysis; DLS, dynamic light scattering; cCCM, complete cell culture medium (RPMI-1640 supplemented with 5% FBS, 2 mM L-alanyl-L-glutamine and 1% antibiotics).

[a] NTA; values are mean ± standard deviation of the particle size distribution.

[b] DLS; values are mean ± standard deviation of the particle size distribution obtained by the CONTIN algorithm (shown is the value for the most representative peak).

[c] ζ potential; samples were centrifuged and redispersed in water (pH neutral) prior to analysis. Values are mean ± standard deviation of three measurements.

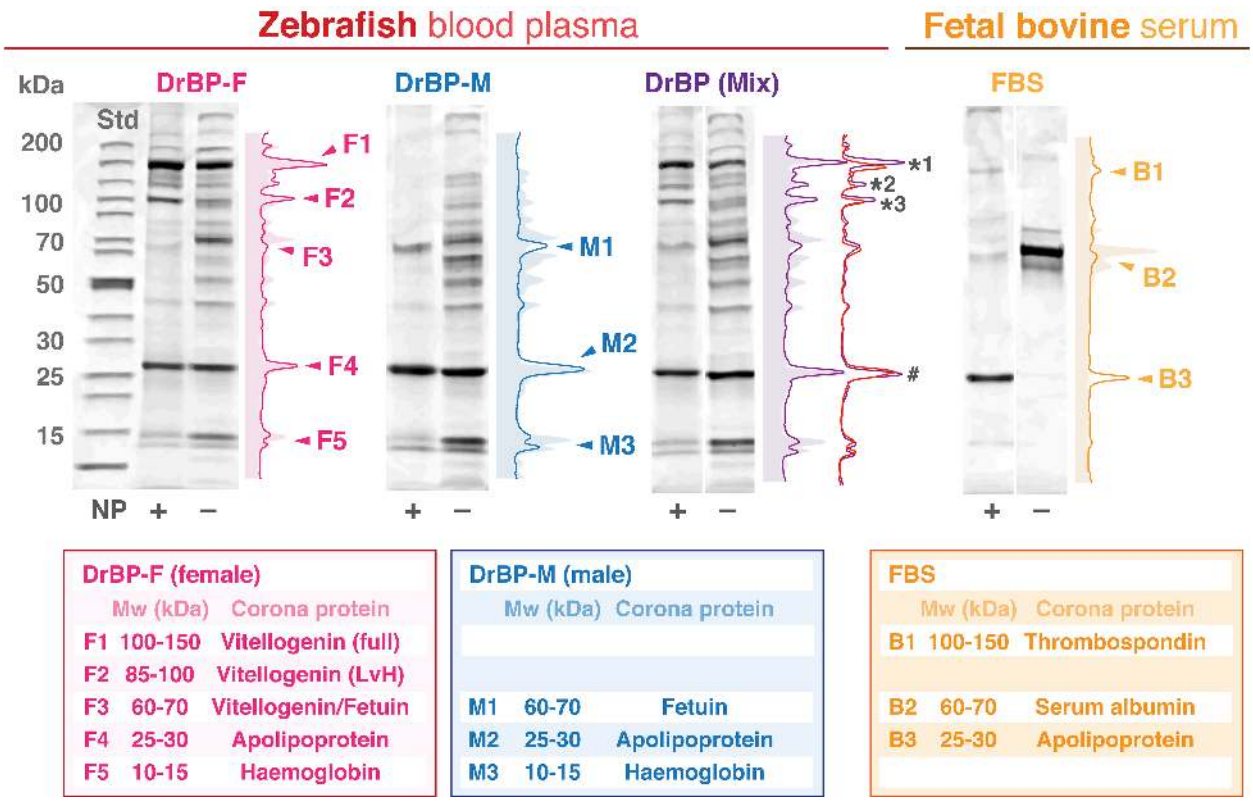


**Figure 1.** Sex- and species-specific biological identity of 70 nm $SiO_2$ nanoparticles. Long-lived, hard protein coronas originated from *Danio rerio* blood plasma (DrBP, F for female and M for male) or FBS were separated by SDS-PAGE and stained with Coomassie Brilliant Blue. Left and right lanes represent corona proteins (NP+) and 5 $\mu$g of total proteins (NP–), respectively. Associated spectra show the intensity profile (NP+, solid lines; NP–, filled space), arrowheads indicating the positions of peaks/bands analysed by tandem mass spectrometry for protein identification. Most representative protein IDs were summarised in the boxes below (See Tables S1† & S2† for more details). The additional spectra in DrBP (Mix) show a quantitative comparison of intensity profiles for corona proteins between DrBP (Mix) (purple line) and a calculated average of DrBP-F and DrBP-M (red line). The numbered asterisks represent vitellogenin peaks that were consistently higher in DrBP (Mix), where *1 = 121 ± 8%, *2 = 132 ± 30%, and *3 = 117 ± 16% (mean ± S.D., $n$ = 3). In contrast, the apolipoprotein A-I peak

indicated by the number sign had 107 ± 6% (mean ± S.D., $n = 3$). A representative gel of three independent experiments is shown (See Fig. S1† for the intact gel image).

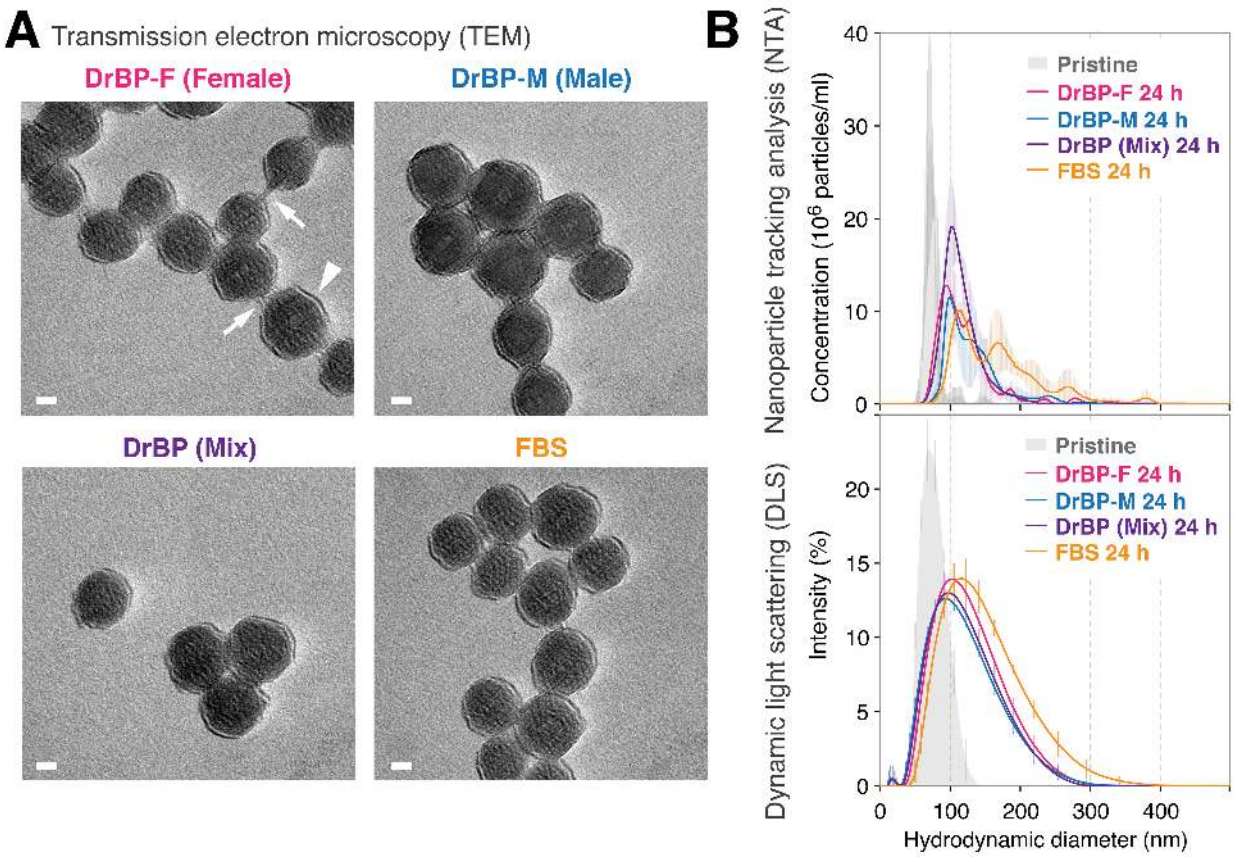


**Figure 2.** Characterisation of $SiO_2$ nanoparticle-protein complexes. (A) TEM images of $SiO_2$ nanoparticle-protein complexes, stained with uranyl acetate for the visualisation of electron-lucent organic layers around nanoparticles (arrowhead). Protein bridges can also be seen in the inter-particle space (arrows), confirming that the electron-lucent layer is not an artefact of over-focusing. Such layers were not observed in the control specimen (uranyl acetate-stained pristine particles). Scale bars = 20 nm. See Fig. S3† for an electron micrograph of pristine $SiO_2$ nanoparticles with associated size statistics. (B) Sizing of $SiO_2$ nanoparticle-protein complexes. The hydrodynamic size distribution was studied by nanoparticle tracking analysis and dynamic light scattering. The filled histograms show the size distribution of pristine $SiO_2$ nanoparticles (nominal size = 70 nm), whereas the solid lines represent the nanoparticle-protein complexes

formed following 24 h incubation with the protein sources denoted. Mean values of three measurements are plotted, and the error bars represent standard deviations.

**Nanoparticle uptake bias in multilineage haematopoietic cells.**

Zebrafish whole kidney marrow (WKM) is a haematopoietic organ analogous to bone marrow in mammals, and houses leukocyte-enriched blood cells having a notably lower fraction of erythrocytes (ca. 40%) than that in blood (>99%).[31] This provides an opportunity not only to simultaneously assess the two lineages of interest – the lymphoid and myeloid populations – but also to preserve inter-cellular communications among the haematopoietic multilineage. As reported elsewhere,[31] the WKM cells consisted of approximately 20% of the lymphoid lineage and a slightly larger fraction of the myeloid lineage (neutrophils, monocyte/macrophages and eosinophils), erythrocytes and lymphoid/myeloid precursors accounting for the rest (Fig. 3). Although erythrocytes did not discretely appear as a clear single population in our flow cytometry setting, the lymphoid and myeloid gates typically embraced a negligible fraction of contaminating erythrocytes (Fig. 3, May-Grünwald/Giemsa staining). We therefore restrict our focus to the two lineages of interest studied herein: lymphoid and myeloid populations.

The myeloid population consists mainly of professional phagocytes such as neutrophils, monocyte/macrophages and dendritic cells.[14, 32] Little is known about nanoparticle uptake by neutrophils and dendritic cells *in vitro*, however, monocultures of monocyte/macrophage lines and primary macrophages are frequently suggested as a potent scavenger of nanoparticles.[33-36] Here we show, as anticipated from their intrinsic capacity for binding/engulfing bacterial particles (*E. coli* BioParticles), that the myeloid population in general accumulated the nanoparticle-protein complexes to a greater extent (up to 2-fold) than the lymphoid population (Fig. 4). In both cases, only less than 25% of the cell population showed high nanoparticle accumulation (binding/uptake) (Fig. S6†); this observation was supported by imaging of the cell populations after post-exposure sorting (Fig. 5). The short exposure duration (2 h) could partly

be an explanation, yet we also believe that this reflects the phenotype heterogeneity of the WKM cells. For example, only 16% of the sorted myeloid population (roughly 4.5% of the total WKM cells) belong to the monocyte/macrophage phenotype (Fig. 3). The limited phagocytic activity in the positive control (*E. coli* BioParticles) additionally suggests that neutrophils, the most abundant scavenger of bacteria, were not activated under the experimental conditions used in this study. The cells in the lymphoid population are morphologically not distinguishable, and thus we do not know what could account for the minor fraction of lymphoid cells that accumulated nanoparticles (<20%). In mammals, the lymphoid lineage assumes the central role in developing adaptive immunity in concert with antigen-presenting cells from the innate immunity arm. Their contribution to immunity against nanoparticles *via* inter-cellular communication has gained attention (reviewed in ref 37), however, their direct interaction with the protein corona around nanoparticles is much less explored. Interestingly, a recent report suggests that B lymphocytes, but not T cells, residing in the liver were capable of accumulating quantum dots *in vivo* in mice.[38] Nonetheless, these observations generally support our previous findings that immune recognition of nanoparticles in this size range (ca. 70 nm) is cell type-dependent, with phagocytes as most proficient for nanoparticle uptake.[6, 39]

**Preferential uptake of nanoparticles with a female biological identity.**

Using the flow cytometric approach, we were able to show the two leukocyte populations are of particular interest in nanoparticle uptake. What we find even more striking is that both populations accumulated nanoparticles significantly more when the protein corona was pre-formed of DrBP-F than of DrBP-M, whereas that of FBS lies somewhere in between the two (Fig. 4). The selected CLSM images exemplify some of those extreme cases; the complexes pre-formed with DrBP-F appear to accumulate greatly around/inside the cells, whereas infrequent

spot-like deposition of small clusters were a common feature for those with DrBP-M and FBS (Fig. 5). The latter suggests a typical pattern of nanoparticle build-up in lysosomes.[40, 41] The massive accumulation shown in the former case would probably represent among the high end of cell-associated FITC fluorescence quantified in flow cytometry, but the precise subcellular localisation of the nanoparticles needs to be further investigated.[42]

In our previous study, silver nanoparticle-protein complexes were pre-formed with serum (-equivalent) proteins of an evolutionary distant species pair (*Eisenia fetida* coelomic proteins and FBS). The corona composition was inherently different between the two: the uniqueness arising from the entirely different repertoire of available proteins.[6] The species-specificity of the corona in this study is rather limited as the repertoire is better conserved between fish and mammals.[16] The protein corona pre-formed of FBS seems to have less protein and is prone to multimeric clustering, yet the compositional profile is somewhat comparable to that of DrBP-M, with the majority being apolipoprotein A-I. The corona pre-formed of DrBP-F or the "female" biological identity, on the other hand, shares a similarity to the male counterpart except for a surplus contribution of vitellogenin. We have considered whether the cellular uptake/binding preference can be modulated depending on the sex of the donor from which the WKM cells were derived. Briefly, we decomposed the dataset to two sets of results, such that cells from female and male fish were exposed to nanoparticles with either "male" or "female" biological identity, respectively. This did not result in a change of the overall picture, indicating that the nanoparticles with a female identity were preferentially accumulated irrespective of the sex of the fish from which the cells were obtained (Fig. S7). Vitellogenin is an inducible protein in male fish upon endocrine disruption (reviewed in ref 43); this signifies that WKM cells from male fish should tolerate and recognise vitellogenin as self, native proteins to them. The protein corona

pre-formed of FBS, or the "non-native" biological identity, could in theory be regarded as exotic in certain scenarios. Possible examples in this study are: the bound proteins do not share sufficient structural homology (e.g. apolipoprotein A-I), or they are simply non-existent in the repertoire (e.g. serum albumin). This raises a possibility for the non-selfness of the biological identity to trigger naïve B cell activation and eventually adaptive immunity (see the review on nanomaterials and adaptive immunity in ref 37). This, however, is not within the scope of our study, as it is unlikely for the B lymphocytes to differentiate into antibody-secreting plasma cells under the given experimental condition. What could then be the true nature of nanoparticles' differential biological identity? From the immunological standpoint, a species-specific biological identity encompasses antigenicity directly recognised by e.g. cognate B-cell receptors and indirectly *via* antigen presentation after nanoparticle uptake. Invertebrate organisms lack such adaptive mechanisms that later flourished during evolution, and we previously suggested that protein coronas made of an exotic repertoire would thus evade innate immune recognition due to the absence of compatible receptors.[6] In this study, despite being self entities, the sex-specificity of nanoparticles' biological identity had a strong influence on cellular accumulation as was the case for the species differences in our previous report.[6] A possible clue to this proposed mystery is that the nanoparticle-bound proteins could also prompt danger signals to alert innate immune systems, coined as nanomaterial-associated molecular patterns or NAMPs.[37] Nanoparticles are known to cause interacting proteins to (partially) denature, and resultant rearrangements of the tertiary structure may expose the buried core (cryptic epitope) of the proteins.[44-47] Proteins may also be locally concentrated at nanoparticles[6] leading to avidity effects, or aggregate in a surface-assisted manner as a result of the loss of native conformation.[48, 49] What we noticed with reference to our previous study[6] and another recent study on bivalves[4] is that the local enrichment

of certain endogenous proteins in the corona may have aided enhanced nanoparticle recognition. In the present study, vitellogenin from DrBP-F was found to be what distinguished the female biological identity from its male counterpart. The molecular mechanisms underlying the detection of nanoparticle-bound vitellogenin and potential immune responses that would follow are yet to be unravelled, however, the immediate implications are that *in vitro* testing employing fish cell lines may require rethinking and careful considerations for the corona proteome to which cells are exposed. This is because it can dictate the toxicokinetics not only due to species differences but also to the sex-specific repertoire of proteins. In fact, established or primary cell lines of fish species have been increasingly used in the toxicity testing of nanomaterials with the canonical practice of choosing FBS as cell culture supplements.[50-54] The structural similarity of vitellogenins to apolipoproteins also suggests their versatility in binding to nanoparticles other than those composed of $SiO_2$. For the extrapolation of this knowledge to *in vivo* studies, care should be taken that the protein concentrations used in this study do not reflect the realistic exposure scenario. This is not only because of the binding kinetics (concentration-dependent) but also due to the possibility of missing rare proteins that might have high affinity for the nanoparticle surface.[55] In addition, vitellogenin production is vital in oviparous animals, and its plasma concentration is dependent on the life history and seasons (reviewed in ref 56). Further complications are introduced by environmental transformation of nanoparticles and the routes of exposure (e.g. gills). Although it is ultimately the blood proteins that the infiltrating nanoparticles may encounter once they translocate to the bloodstream, the concentration and the chemical/physical state of the nanoparticles are very likely different from what were used in this study. What we could learn nevertheless in the context of *in vivo* extrapolation is a possibility for specific targeting of nanoparticles to developing oocytes equipped with vitellogenin receptors as

well as potential downstream consequences. This in turn could be prevented by leukocytes that are capable of removing such nanoparticle-protein complexes from the bloodstream.

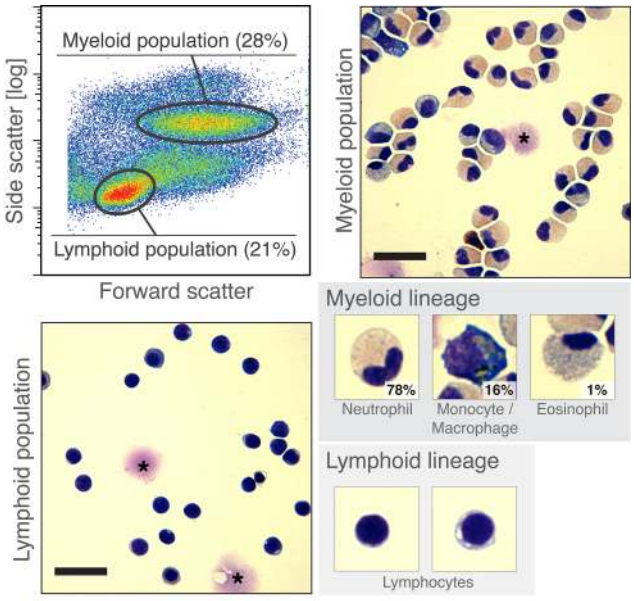


**Figure 3.** Lymphoid and myeloid populations of zebrafish whole kidney marrow (WKM) cells. Top-left panel shows light scatter-based cell typing in flow cytometry. A representative density plot is shown. Lymphoid and myeloid populations can be gated in the $FS^{low}/SS^{low}$ and $FS^{high}/SS^{high}$ clusters, respectively. Other recorded events represent precursor cells ($FS^{high}/SS^{low}$) and erythrocytes (scattered all over in the FS/SS profile). The WKM cells were sorted accordingly and their morphology was imaged after May-Grünwald/Giemsa staining. Weak purple stains (asterisks) are staining artefacts. For the myeloid population, occurrence of each identified cell type (in percentage, $n = 1584$) is indicated in the close-up images (boxes, size = $15 \times 15\ \mu m^2$). Scale bars = $20\ \mu m$. FS, forward scatter; SS, side scatter.

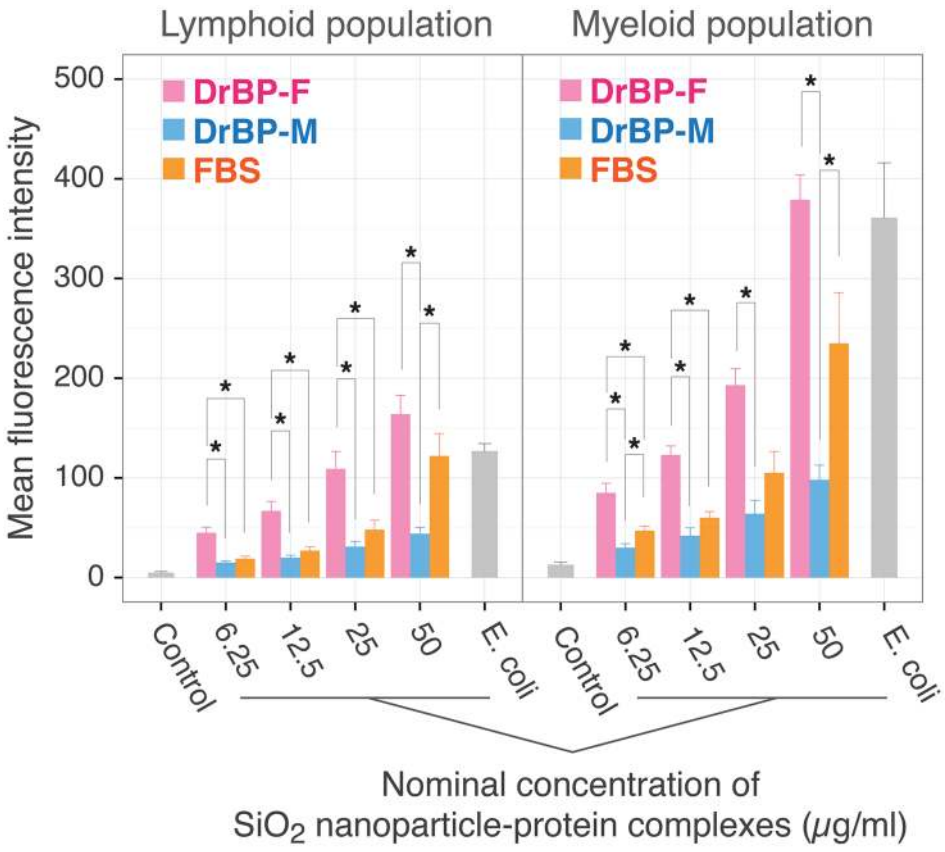


**Figure 4.** Cellular accumulation of $SiO_2$ nanoparticle-protein complexes pre-formed with three different protein corona types. Mean fluorescence intensity of lymphoid and myeloid populations reflects membrane-adhered and internalised 70 nm $SiO_2$ nanoparticles (labelled with FITC). *E. coli* BioParticles (10 bacteria per cell, non-opsonised) were included as a positive control for uptake/binding. Values are mean ± SE of six independent assays. Asterisk denotes a significant difference (One-way ANOVA, Tukey's HSD, $p < 0.05$) between the three protein corona types at each test concentration. For a representative profile of the fluorescence intensity distribution, see Fig. S6†.

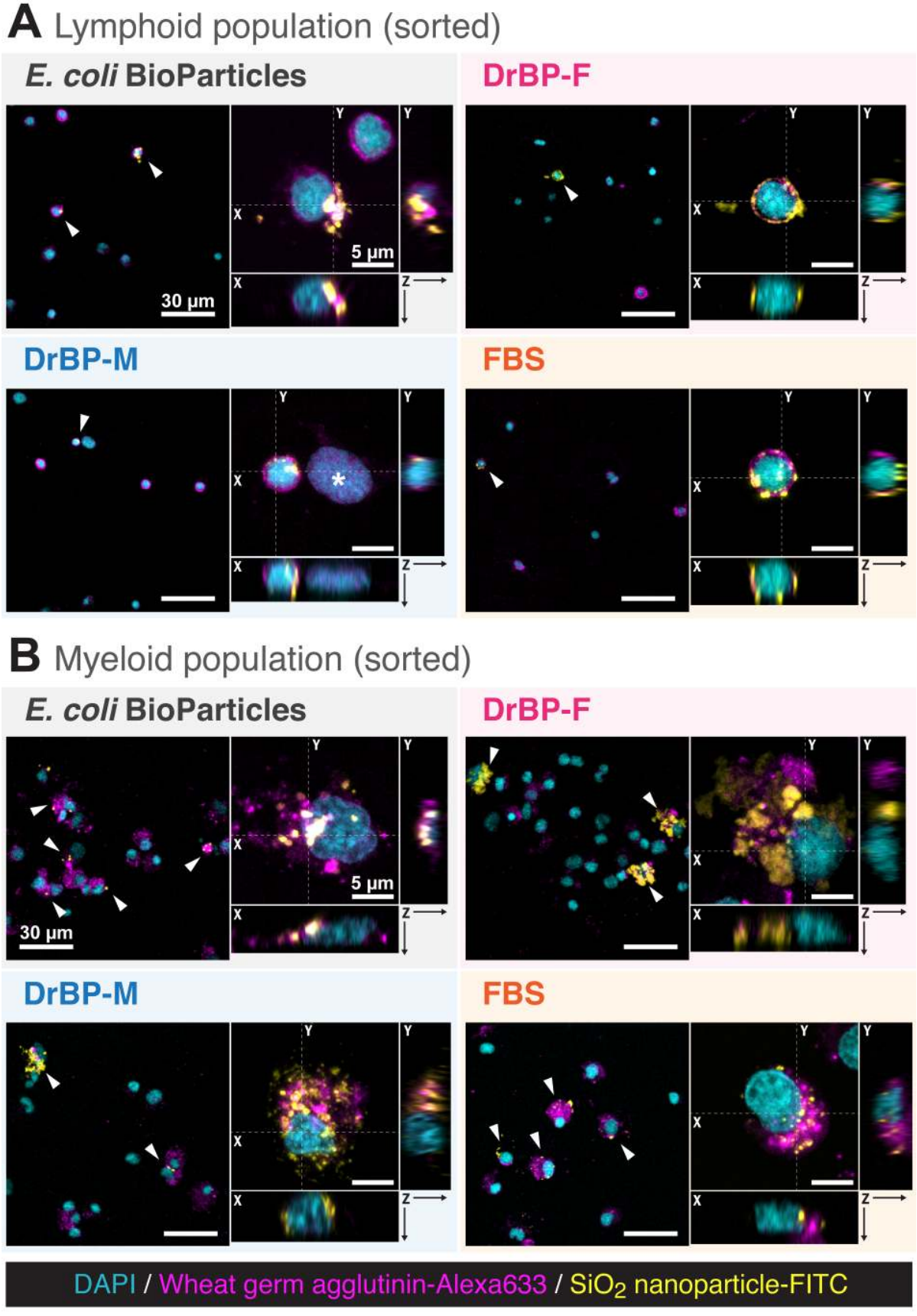
A Lymphoid population (sorted)
E. coli BioParticles
DrBP-F
DrBP-M
FBS
30 μm
5 μm
B Myeloid population (sorted)
E. coli BioParticles
DrBP-F
DrBP-M
FBS
30 μm
5 μm
DAPI / Wheat germ agglutinin-Alexa633 / SiO2 nanoparticle-FITC

**Figure 5.** Confocal laser scanning microscopy images of (A) the lymphoid population and (B) the myeloid population following post-exposure sorting of the two populations. Zebrafish WKM cells were exposed to $SiO_2$ nanoparticle-protein complexes pre-formed with three different protein corona types (2 h, 50 $\mu$g/ml), after which the two subpopulations were formalin-fixed, stained, and sorted prior to confocal imaging. Wheat germ agglutinin (WGA) stains cellular components that are glycosylated (specific for *N*-acetylglucosaminyl and sialic acid residues) while DAPI stains the nuclei. Each panel consists of two images: a low magnification image on the left (scale bar = 30 $\mu$m) and a high magnification image on the right (scale bar = 5 $\mu$m) along with an orthogonal view (the xz and yz planes). White arrowheads in the low magnification image indicate association of the fluorescent particles with cells. Asterisk denotes a contaminating proerythroblast. The brightness/contrast setting was adjusted per image in order to optimally visualise (sub-)cellular localisation of nanoparticles. Colour legends are shown at the bottom.

## Conclusions

To the best of our knowledge, we here report for the first time the differential cellular uptake of nanoparticles with a sex-specific biological identity that could be acquired within the same species. The basis for this observation stems from the variation in the protein repertoire, and this simple cause-effect relationship should in principle be applicable to other model organisms, not limited to zebrafish. The female biological identity was preferentially recognised by leukocytes, however, we would not hastily extrapolate this observation to higher organisms like mammals. This is because we believe it is the local build-up of certain endogenous proteins at nanoparticles that could prime immune recognition, rather than a simple compositional, sex-specific uniqueness of the corona proteome. For example, in the case of human blood plasma-derived protein coronas, future studies may benefit from identification of uniquely enriched proteins specific for certain (patho-)physiological conditions.[10] The concept of repertoire differences in the corona proteome therefore deserves further attention, as various factors such as sex-specific biological conditions exemplified in this study could alter the nanoparticle-cell interactions.

## Author contributions

Y.H. conceived, designed and supervised the overall project. T.M. performed NTA and TEM experiments. Y.H. and S.M. performed DLS and SDS-PAGE experiments. Y.H. conducted flow cytometry, cell sorting and staining experiments. Y.H. and M.T. performed CLSM experiments. C.S. and J.J.E. performed mass spectrometry. Y.H. and K.K.S. developed the blood collection method. U.S., C.O., C.W. supervised biological experiments using zebrafish. D.S.S. supervised characterisation experiments and the overall project. Y.H. performed analysis of all characterisation, imaging and biological data and wrote the manuscript.

## Corresponding Authors

* Phone: +45 8715 4917 (Y. H.); +45 2338 5789 (D. S.). e-mail: yuya.hayashi@mbg.au.dk (Y. H.); duncan@inano.au.dk (D. S.).

## Acknowledgements

We gratefully acknowledge the fish facilities at Karlsruhe Institute of Technology (KIT) and Aarhus University for zebrafish husbandry. We also thank Thomas Boesen at iNANO, Aarhus University, for his technical help with TEM, Wilko Thiele and Marina Mione at the Institute of Toxicology and Genetics, Karlsruhe Institute of Technology (KIT), for their assistance in cell sorting and haematology staining, and Péter Engelmann at Department of Immunology and Biotechnology, University of Pécs, for his insightful comments on the manuscript. The present work was financially supported by the Danish Council for Independent Research | Technology and Production Sciences (FTP) through the individual postdoctoral grant 4093-00137B "DANiim – *Danio rerio* (zebrafish) Innate Immunity Model for Bionanoscience" (Y. H.).

**References**


1. G. V. Lowry, K. B. Gregory, S. C. Apte and J. R. Lead, *Environ. Sci. Technol.*, 2012, **46**, 6893-6899.
2. M. P. Monopoli, C. Aberg, A. Salvati and K. A. Dawson, *Nat. Nanotechnol.*, 2012, **7**, 779-786.
3. F. Nasser and I. Lynch, *J. Proteomics.*, 2016, **137**, 45-51.
4. L. Canesi, C. Ciacci, R. Fabbri, T. Balbi, A. Salis, G. Damonte, K. Cortese, V. Caratto, M. P. Monopoli, K. Dawson, E. Bergami and I. Corsi, *Environ. Res.*, 2016, **150**, 73-81.
5. Y. Hayashi, T. Miclaus, P. Engelmann, H. Autrup, D. S. Sutherland and J. J. Scott-Fordsmand, *Nanotoxicology*, 2016, **10**, 303-311.
6. Y. Hayashi, T. Miclaus, C. Scavenius, K. Kwiatkowska, A. Sobota, P. Engelmann, J. J. Scott-Fordsmand, J. J. Enghild and D. S. Sutherland, *Environ. Sci. Technol.*, 2013, **47**, 14367-14375.
7. D. Docter, D. Westmeier, M. Markiewicz, S. Stolte, S. K. Knauer and R. H. Stauber, *Chem. Soc. Rev.*, 2015, **44**, 6094-6121.
8. P. d. Pino, B. Pelaz, Q. Zhang, P. Maffre, G. U. Nienhaus and W. J. Parak, *Mater. Horiz.*, 2014, **1**, 301-313.
9. Philipp E. Geyer, Nils A. Kulak, G. Pichler, Lesca M. Holdt, D. Teupser and M. Mann, *Cell Systems*, 2016, **2**, 185-195.
10. M. J. Hajipour, S. Laurent, A. Aghaie, F. Rezaee and M. Mahmoudi, *Biomater. Sci.*, 2014, **2**, 1210-1221.
11. F. Babaei, R. Ramalingam, A. Tavendale, Y. Liang, L. S. K. Yan, P. Ajuh, S. H. Cheng and Y. W. Lam, *J. Proteome Res.*, 2013, **12**, 1580-1590.

12. J. Schindelin, I. Arganda-Carreras, E. Frise, V. Kaynig, M. Longair, T. Pietzsch, S. Preibisch, C. Rueden, S. Saalfeld, B. Schmid, J.-Y. Tinevez, D. J. White, V. Hartenstein, K. Eliceiri, P. Tomancak and A. Cardona, *Nat. Methods*, 2012, **9**, 676-682.

13. C. A. Schneider, W. S. Rasband and K. W. Eliceiri, *Nat. Methods*, 2012, **9**, 671-675.

14. V. Wittamer, J. Y. Bertrand, P. W. Gutschow and D. Traver, *Blood*, 2011, **117**, 7126-7135.

15. S. K. Singh, S. Sethi, S. Aravamudhan, M. Krüger and C. Grabher, *PLoS One*, 2013, **8**, e73998.

16. C. Li, X. F. Tan, T. K. Lim, Q. Lin and Z. Gong, *Sci. Rep.*, 2016, **6**, 24329.

17. T. Miclăuş, V. E. Bochenkov, R. Ogaki, K. A. Howard and D. S. Sutherland, *Nano Lett.*, 2014, **14**, 2086-2093.

18. M. P. Monopoli, D. Walczyk, A. Campbell, G. Elia, I. Lynch, F. Baldelli Bombelli and K. A. Dawson, *J. Am. Chem. Soc.*, 2011, **133**, 2525-2534.

19. R. N. Finn, *Biol. Reprod.*, 2007, **76**, 926-935.

20. M. Hausler, C. Schafer, C. Osterwinter and W. Jahnen-Dechent, *Pediatr. Res.*, 2009, **66**, 660-664.

21. S. Tenzer, D. Docter, J. Kuharev, A. Musyanovych, V. Fetz, R. Hecht, F. Schlenk, D. Fischer, K. Kiouptsi, C. Reinhardt, K. Landfester, H. Schild, M. Maskos, S. K. Knauer and R. H. Stauber, *Nat. Nanotechnol.*, 2013, **8**, 772-781.

22. S. Tenzer, D. Docter, S. Rosfa, A. Wlodarski, J. Kuharev, A. Rekik, S. K. Knauer, C. Bantz, T. Nawroth, C. Bier, J. Sirirattanapan, W. Mann, L. Treuel, R. Zellner, M. Maskos, H. Schild and R. H. Stauber, *ACS Nano*, 2011, **5**, 7155-7167.

23. R. Cukalevski, M. Lundqvist, C. Oslakovic, B. Dahlbäck, S. Linse and T. Cedervall, *Langmuir*, 2011, **27**, 14360-14369.

24. K. Saha, M. Rahimi, M. Yazdani, S. T. Kim, D. F. Moyano, S. Hou, R. Das, R. Mout, F. Rezaee, M. Mahmoudi and V. M. Rotello, *ACS Nano*, 2016, **10**, 4421-4430.

25. C. D. Walkey, J. B. Olsen, F. Song, R. Liu, H. Guo, D. W. H. Olsen, Y. Cohen, A. Emili and W. C. W. Chan, *ACS Nano*, 2014, **8**, 2439-2455.

26. U. Sakulkhu, L. Maurizi, M. Mahmoudi, M. Motazacker, M. Vries, A. Gramoun, M.-G. Ollivier Beuzelin, J.-P. Vallee, F. Rezaee and H. Hofmann, *Nanoscale*, 2014, **6**, 11439-11450.

27. E. Hellstrand, I. Lynch, A. Andersson, T. Drakenberg, B. Dahlbäck, K. A. Dawson, S. Linse and T. Cedervall, *FEBS J.*, 2009, **276**, 3372-3381.

28. C. D. Walkey and W. C. W. Chan, *Chem. Soc. Rev.*, 2012, **41**, 2780-2799.

29. T. Cedervall, L.-A. Hansson, M. Lard, B. Frohm and S. Linse, *PLoS One*, 2012, **7**, e32254.

30. T. Miclăuş, C. Beer, J. Chevallier, C. Scavenius, V. E. Bochenkov, J. J. Enghild and D. S. Sutherland, *Nat. Commun.*, 2016, **7**, 11770.

31. D. Traver, B. H. Paw, K. D. Poss, W. T. Penberthy, S. Lin and L. I. Zon, *Nat. Immunol.*, 2003, **4**, 1238-1246.

32. G. Lugo-Villarino, K. M. Balla, D. L. Stachura, K. Bañuelos, M. B. F. Werneck and D. Traver, *Proc. Natl. Acad. Sci. USA*, 2010, **107**, 15850-15855.

33. O. Lunov, T. Syrovets, C. Loos, J. Beil, M. Delacher, K. Tron, G. U. Nienhaus, A. Musyanovych, V. Mailänder, K. Landfester and T. Simmet, *ACS Nano*, 2011, **5**, 1657-1669.

34. T. dos Santos, J. Varela, I. Lynch, A. Salvati and K. A. Dawson, *Small*, 2011, **7**, 3341-3349.

35. C. D. Walkey, J. B. Olsen, H. Guo, A. Emili and W. C. W. Chan, *J. Am. Chem. Soc.*, 2012, **134**, 2139-2147.

36. A. França, P. Aggarwal, E. V. Barsov, S. V. Kozlov, M. A. Dobrovolskaia and Á. González-Fernández, *Nanomed.*, 2011, **6**, 1175-1188.

37. C. Farrera and B. Fadeel, *Eur. J. Pharm. Biopharm.*, 2015, **95, Part A**, 3-12.

38. K. M. Tsoi, S. A. MacParland, X.-Z. Ma, V. N. Spetzler, J. Echeverri, B. Ouyang, S. M. Fadel, E. A. Sykes, N. Goldaracena, J. M. Kaths, J. B. Conneely, B. A. Alman, M. Selzner, M. A. Ostrowski, O. A. Adeyi, A. Zilman, I. D. McGilvray and W. C. W. Chan, *Nat. Mater.*, 2016, **15**, 1212-1221.

39. Y. Hayashi, P. Engelmann, R. Foldbjerg, M. Szabó, I. Somogyi, E. Pollák, L. Molnár, H. Autrup, D. S. Sutherland, J. Scott-Fordsmand and L.-H. Heckmann, *Environ. Sci. Technol.*, 2012, **46**, 4166-4173.

40. A. Lesniak, A. Campbell, M. P. Monopoli, I. Lynch, A. Salvati and K. A. Dawson, *Biomaterials*, 2010, **31**, 9511-9518.

41. F. Wang, L. Yu, M. P. Monopoli, P. Sandin, E. Mahon, A. Salvati and K. A. Dawson, *Nanomed. Nanotech. Biol. Med.*, 2013, **9**, 1159-1168.

42. M. Al-Rawi, S. Diabaté and C. Weiss, *Arch. Toxicol.*, 2011, **85**, 813-826.

43. H. Segner, *Comp. Biochem. Physiol. C Toxicol. Pharmacol.*, 2009, **149**, 187-195.

44. G. M. Mortimer, N. J. Butcher, A. W. Musumeci, Z. J. Deng, D. J. Martin and R. F. Minchin, *ACS Nano*, 2014, **8**, 3357-3366.

45. Z. J. Deng, M. Liang, M. Monteiro, I. Toth and R. F. Minchin, *Nat. Nanotechnol.*, 2011, **6**, 39-44.

46. P. M. Kelly, C. Åberg, E. Polo, A. O'Connell, J. Cookman, J. Fallon, KrpetićŽeljka and K. A. Dawson, *Nat. Nanotechnol.*, 2015, **10**, 472-479.

47. M. C. Lo Giudice, L. M. Herda, E. Polo and K. A. Dawson, *Nat. Commun.*, 2016, **7**, 13475.

48. A. A. Shemetov, I. Nabiev and A. Sukhanova, *ACS Nano*, 2012, **6**, 4585-4602.

49. S. Linse, C. Cabaleiro-Lago, W.-F. Xue, I. Lynch, S. Lindman, E. Thulin, S. E. Radford and K. A. Dawson, *Proc. Natl. Acad. Sci. USA*, 2007, **104**, 8691-8696.

50. Y. Yue, R. Behra, L. Sigg, P. Fernández Freire, S. Pillai and K. Schirmer, *Nanotoxicology*, 2015, **9**, 54-63.

51. J. P. Wise, B. C. Goodale, S. S. Wise, G. A. Craig, A. F. Pongan, R. B. Walter, W. D. Thompson, A.-K. Ng, A.-M. Aboueissa, H. Mitani, M. J. Spalding and M. D. Mason, *Aquat. Toxicol.*, 2010, **97**, 34-41.

52. N. T. K. Vo, M. R. Bufalino, K. D. Hartlen, V. Kitaev and L. E. J. Lee, *In Vitro Cell. Dev. Biol. Anim.*, 2014, **50**, 427-438.

53. M. L. Fernández-Cruz, T. Lammel, M. Connolly, E. Conde, A. I. Barrado, S. Derick, Y. Perez, M. Fernandez, C. Furger and J. M. Navas, *Nanotoxicology*, 2013, **7**, 935-952.

54. Y. Yue, R. Behra, L. Sigg, M. J. F. Suter, S. Pillai and K. Schirmer, *Environ. Sci. Nano*, 2016, **3**, 1174-1185.

55. C. Fedeli, D. Segat, R. Tavano, L. Bubacco, G. De Franceschi, P. P. de Laureto, E. Lubian, F. Selvestrel, F. Mancin and E. Papini, *Nanoscale*, 2015, **7**, 17710-17728.

56. A. Hara, N. Hiramatsu and T. Fujita, *Fish. Sci.*, 2016, **82**, 187-202.

## Electronic supplementary information

# Female *versus* male biological identities of nanoparticles determine the interaction with the immune system in fish

Yuya Hayashi,*[abc] Teodora Miclaus,[cd] Sivakumar Murugadoss,[b] Masanari Takamiya,[b] Carsten Scavenius,[a] Kasper Kjaer-Sorensen,[a] Jan J. Enghild,[a] Uwe Strähle,[b] Claus Oxvig,[a] Carsten Weiss[b] and Duncan S. Sutherland*[c]

[a.] Department of Molecular Biology and Genetics, Aarhus University, Gustav Wieds Vej 10, 8000 Aarhus C, Denmark
[b.] Institute of Toxicology and Genetics, Karlsruhe Institute of Technology (KIT), Hermann-von-Helmholtz-Platz 1, 76344 Eggenstein-Leopoldshafen, Germany
[c.] iNANO Interdisciplinary Nanoscience Center, Aarhus University, Gustav Wieds Vej 14, 8000 Aarhus C, Denmark
[d.] Nano4Environment Unit, Department of Life Science, INL International Iberian Nanotechnology Laboratory, Avenida Mestre Jose Veiga s/n, 4715-330 Braga, Portugal

* Corresponding authors
Phone: +45 8715 4917 (Y. H.); +45 2338 5789 (D. S.).
e-mail: yuya.hayashi@mbg.au.dk (Y. H.); duncan@inano.au.dk (D. S.).

Number of pages (including the cover page): 15
Number of tables: 2 (in the separate PDF file "Supplementary Tables")
Number of figures: 7

**Table of Contents**

## Supplemental description of experimental methods

*Collection of zebrafish blood plasma*

To obtain a large volume of blood from each fish, a centrifuge-based method reported by Babaei and colleagues[1] was employed with modifications to accommodate large-sized fish. Briefly, fish were first anesthetised with 0.02% tricaine (3-amino benzoic acid ethyl ester) and euthanised in ice-water. Prior to blood harvesting, a custom-made 1.5 ml microcentrifuge tube (Eppendorf) with its bottom excised was suspended in a 13 ml polypropylene tube (Sarstedt), kept on ice and rinsed with anticoagulation buffer prepared of PBS containing 10 mM EDTA (BioUltra, Sigma-Aldrich) and a mixture of 100 U/mL penicillin and 100 μg/mL streptomycin (Gibco). Each euthanised fish had its tail amputated, the wound dipped in the anticoagulation buffer and placed in the upper column of the double tube assembly, before being centrifuged at 40*g* for 5 min at 11°C. Centrifugation was repeated after the second excision as described,[1] and the blood collected was transferred to a Protein LoBind tube (Eppendorf) and spun at 13800*g* for 15 min at 8°C. If haemolysis was apparent, the tube was discarded. The clear supernatant (plasma) was pooled and stored at -80°C until use (within a month). Total protein concentration was quantified by the Bradford assay (Pierce Coomassie Plus, ThermoScientific) with a VersaMax ELISA Microplate Reader (Molecular Devices) following the manufacturer's instructions (absorbance at 595 nm). Normally 6 female or male fish were sacrificed in one session and each batch of pooled plasma had a typical protein yield of 100-200 μg per fish. The blood plasma thus obtained was named DrBP-F or DrBP-M (*Danio rerio* blood plasma - female or male, respectively). DrBP (Mix) is a 1:1 mixture of the two.

*Incubation of $SiO_2$ nanoparticles to form nanoparticle-protein complexes*

The protein concentrations of the DrBP series (DrBP-F, DrBP-M, DrBP-Mix) and FBS (Sigma) were adjusted to 1 mg/ml and 2 mg/ml, respectively, using the anticoagulant buffer. The protein solutions were centrifuged at 16000*g* for 3 min at room temperature (RT) to remove any insoluble protein aggregates, and the supernatants were then incubated with the $SiO_2$ nanoparticles (200 μg/ml) for 24 h in darkness at 26°C. To minimize non-specific binding of proteins to the tube wall, Protein Lobind tubes were used in all steps of incubation and centrifugal isolation of nanoparticle-protein complexes (described below). For the given mass concentration of 70 nm $SiO_2$ nanoparticles (200 μg/ml), nanoparticle number and outer surface area can be roughly calculated to be $6\times10^{11}$/ml and 86 $cm^2$/ml,

respectively. Based on these numbers we can then assume the minimal number of serum albumin molecules that are necessary to completely cover the nanoparticle surface.[2] To ensure a full surface coverage, an excess of proteins accounting for theoretical 5 layers has been recommended.[3] In this study, protein concentrations used for incubation correspond to approximately 2.5-5.0% of the original protein concentrations in whole blood/serum and were 1 mg/ml (the DrBP series) and 2 mg/ml (FBS). The selection of candidate concentrations was further short-listed by the dispersibility of the nanoparticle pellet after centrifugation, as analysed by dynamic light scattering (described below). At the chosen ratio of nanoparticles-to-proteins, theoretically, there is a 22 (the DrBP series) or 44 (FBS) times excess of proteins, enough to cover the nanoparticle surface.

*Centrifugal isolation*

The nanoparticle-protein complexes were isolated from unbound and loosely-bound proteins by a well-established centrifugation technique as described previously.[4] Briefly, after pelleting the nanoparticle-protein complexes by centrifugation at 16000*g* for 20 min at 21°C, the pellet was redispersed in PBS and centrifuged again. This washing process was repeated three times (the suspension was transferred to a new Protein Lobind tube after the second wash), before concentrated SDS-loading buffer (with 100 mM dithothreitol as a reducing agent; 5X Lane Marker Reducing Sample Buffer, ThermoScientific) was added to the nanoparticle pellet. The samples were heated at 98°C for 5 min to denature the proteins and strip off the hard protein corona from the nanoparticles, after which the nanoparticles were spun down at 16000*g* for 30 min at 4 °C and the supernatant was stored at -20°C until analysis. Nanoparticle-free blanks were separately prepared and we confirmed by SDS-PAGE that no protein aggregates were unintentionally spun down during the centrifugal isolation steps.

*Sodium dodecyl sulfate polyacrylamide gel electrophoresis (SDS-PAGE)*

The hard corona protein samples were diluted with PBS to adjust the SDS-loading buffer concentration, and for reference total protein samples were prepared by heating respective protein solutions (5 μg) in the presence of the SDS-loading buffer. The denatured proteins were separated by 4-20% gradient SDS-PAGE (Precise Protein Gels, ThermoScientific) along with a PageRuler Unstained Protein Ladder (ThermoScientific) as the molecular weight standard (10-200 kDa). Protein bands in the gels were detected by Imperial Protein Stain (Coomassie Brilliant Blue staining with sensitivity of 3 ng; ThermoScientific) following the manufacturer's instructions. The stained gels were scanned on an

Odyssey infrared imager (Li-Cor) and the images were processed with Fiji/ImageJ.[5, 6] For analysis, the plot profile tool was used to quantify the staining intensity and run length. The whole process starting from the formation of the nanoparticle-protein complexes to documentation of the stained gels was repeated three times to ensure reproducibility.

*Mass spectrometry (MS)*

In-gel digestion of selected proteins was performed essentially as described previously.[4] The tryptic peptides were micro-purified using C18 stage tips (Proxeon, ThermoScientific). Nano-electrospray ionization MS/MS (nanoESI-MS/MS) analyses were performed on an EASY-nLC II system (ThermoScientific) connected to a TripleTOF 5600+ mass spectrometer (AB SCIEX) equipped with a NanoSpray III source (AB SCIEX) operated under Analyst TF 1.6 control. The trypsin-digested samples were suspended in 0.1% formic acid, injected, trapped and desalted isocratically on a precolumn (ReproSil-Pur C18-AQ 3 μm resin, Dr. Maisch GmbH, Germany). The peptides were eluted and separated on a 15 cm analytical column (75 μm i.d.), pulled in-house (P2000 laser puller, Sutter Instrument), and packed with ReproSil-Pur C18-AQ 3 μm resin (Dr. Maisch GmbH, Germany). Peptides were eluted from the analytical column at a flow rate of 250 nL/min using a 30 min gradient from 5% to 35% of solution B (0.1% formic acid, 100% acetonitrile). The collected MS files were converted to Mascot generic format (MGF) using the AB SCIEX MS Data Converter beta 1.1 (AB SCIEX) and the "protein pilot MGF" parameters. The generated peak lists were searched using an in-house Mascot search engine (Matrix Science). Search parameters were allowing one missed trypsin cleavage site and propionamide as a fixed modification with peptide tolerance and MS/MS tolerance set to 20 ppm and 0.4 Da, respectively.

*Transmission electron microscopy (TEM)*

The primary particle size distribution of the $SiO_2$ nanoparticles was examined under a Phillips CM20 transmission electron microscope operating at 200 keV. To establish a size distribution ($n \geq 1000$) from several TEM images across the grid, the scanning probe image software SPIP (Image Metrology, Denmark) was used. For imaging of the $SiO_2$ nanoparticle-protein complexes, the complexes were prepared as described above except that they were washed with MilliQ water (18.2 MΩ) instead of PBS for desalting purposes. A drop of the colloids was directly deposited onto an oxygen plasma-treated copper grid with a formvar/carbon membrane (Ted Pella, CA) and left for 1 minute. The excess liquid

was wipe-dried and a drop of freshly prepared uranyl acetate aqueous solution (1% w/v) was applied to stain the specimen. After 1 minute, the excess contrast agent solution was dried-off in a similar manner.

*Nanoparticle tracking analysis (NTA)*

The hydrodynamic size distribution of $SiO_2$ nanoparticle-protein complexes was assessed using a NanoSight LM10-HS (Malvern Instruments, UK) instrument with a laser wavelength of 405 nm. Prior to analysis each sample was diluted in sterile-filtered PBS (or MilliQ water for the pristine sample) in order to have a working concentration of ca. $10^8$ nanoparticles/ml. Three videos of 90 seconds each were recorded and processed individually (NanoSight NTA 2.3 build 025). To avoid cross-contamination, the measurement cell was flushed with the diluent after each measurement. Signal-to-noise ratio was high enough to confidently differentiate light scattering of $SiO_2$ nanoparticles from that of proteins and, if any, protein aggregates.

*Dynamic light scattering (DLS) and zeta potential analysis*

Light scattering analysis of the $SiO_2$ nanoparticle-protein complexes was performed on a Malvern ZetasizerNano (Malvern Instruments, UK) with the laser wavelength of 633 nm. For DLS, a detection angle at 173° was used and the correlation function obtained was fitted to a multiple exponential model (CONTIN algorithm) using the Zetasizer Software 7.11 (Malvern Instruments, UK). In comparison to NTA, DLS allows sizing of $SiO_2$ nanoparticles at concentrations relevant for *in vitro* cell assays (50-200 μg/ml) in the presence of proteins provided that contribution of the proteins to light scattering is negligible. The $SiO_2$ nanoparticle-protein complexes were thus further studied following redispersion and 2 h additional incubation in complete cell culture medium (cCCM; details described below). For zeta potential measurements, the $SiO_2$ nanoparticle-protein complexes with or without the 2 h additional incubation in cCCM were desalted (pelleted and redispersed in MilliQ water) and the electrophoretic mobility was immediately analysed. For the calculation of zeta potentials the Henry equation was applied with the Smoluchowski approximation ($f(\kappa a) = 1.5$) using the Malvern's software.

## Intact image of the gel used in Figure 1 (Fig. S1)

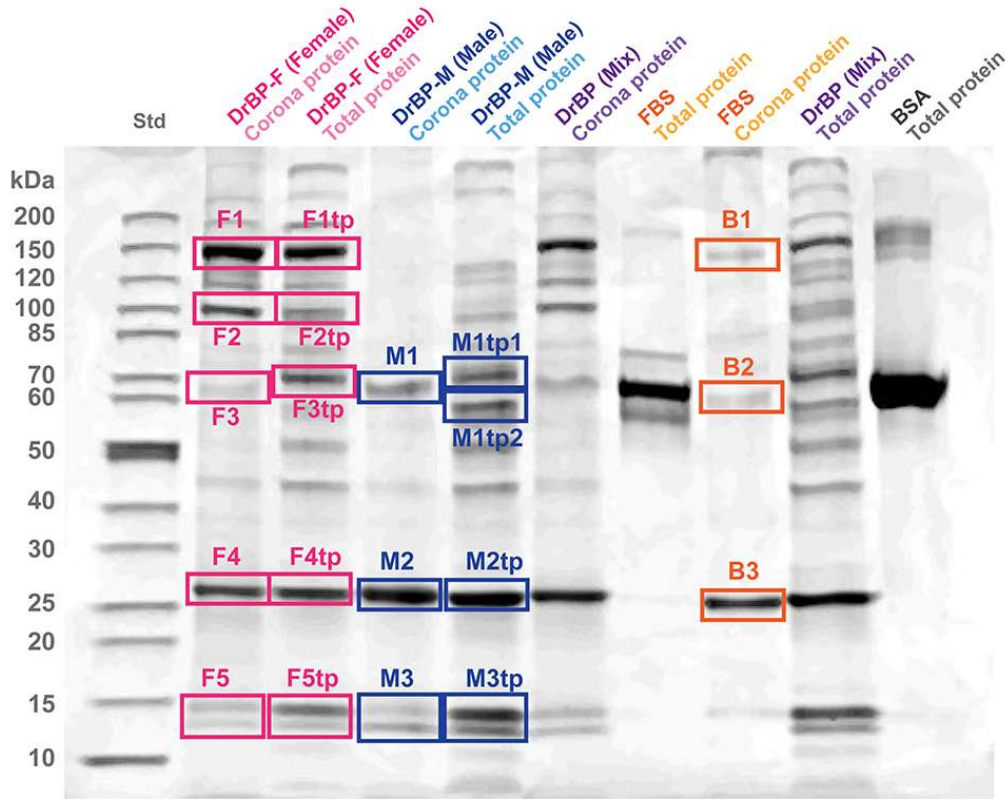


**Figure S1.** The intact image of the Coomassie Brilliant Blue-stained gel shown in Figure 1. Boxes denote the positions of each band excised for tandem mass spectrometry analysis. A unique band ID was assigned to each box. See Tables S1 & S2 for proteins identified for each band ID (Supplementary Tables).

## Sequence coverage maps for vitellogenin 1 (Fig. S2)


**Figure S2.** Sequence coverage maps for vitellogenin 1 (Q1LWN2) identified by tandem mass spectrometry. See Figure S1 for the band positions of F1, F2 and F4. The F1 band corresponds to the theoretical molecular weight of full-length vitellogenin 1 (148 kDa), F2 the cleaved product lipovitellin heavy chain (114 kDa), and F4 another cleaved product lipovitellin light chain (26 kDa). See the review by Finn (2007)[7] for details of the molecular mass prediction for vitellogenins.

## TEM image of pristine $SiO_2$ nanoparticles (Fig. S3)

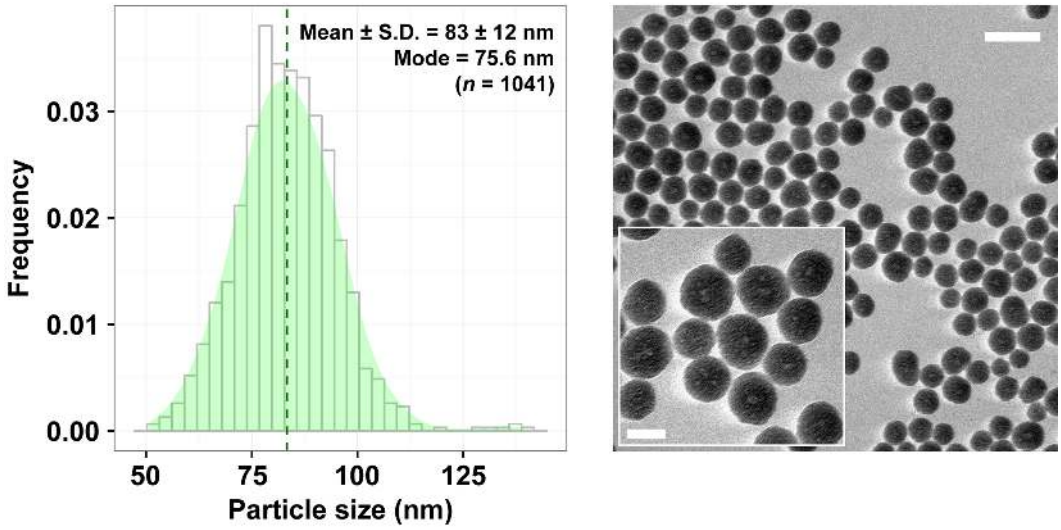


**Figure S3.** Electron micrographs of $SiO_2$ nanoparticles. A TEM image of pristine nanoparticles with associated size statistics. Scale bars = 200 nm and 50 nm (inset).

## Colloidal stability under the exposure condition (Fig. S4)

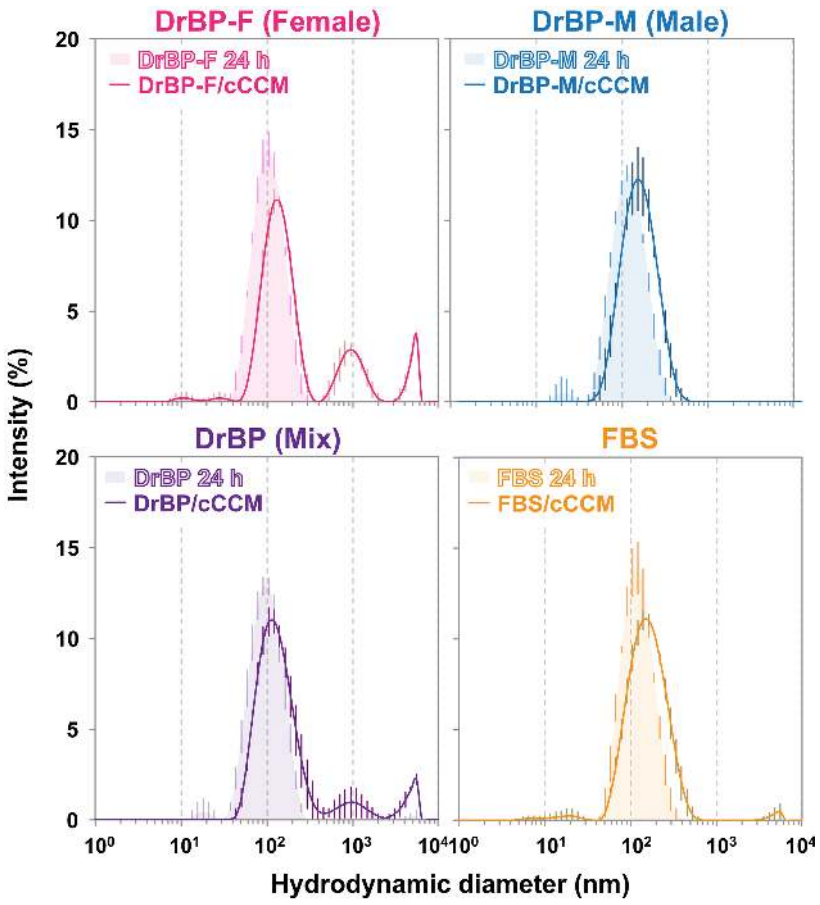


**Figure S4.** Colloidal stability of $SiO_2$ nanoparticle-protein complexes under the exposure condition (2 h incubation at 26°C in cCCM). The filled histograms and solid lines show the size distribution of the complexes before and after the 2 h incubation, respectively. Note that shown are light scatter intensity-based size distributions; the minor peaks in the $\mu$m range are negligible in volume or number. Mean values of three measurements are plotted, and the error bars represent standard deviations. cCCM, complete cell culture medium (containing 5% FBS).

## Protein corona profiles under the exposure condition (Fig. S5)

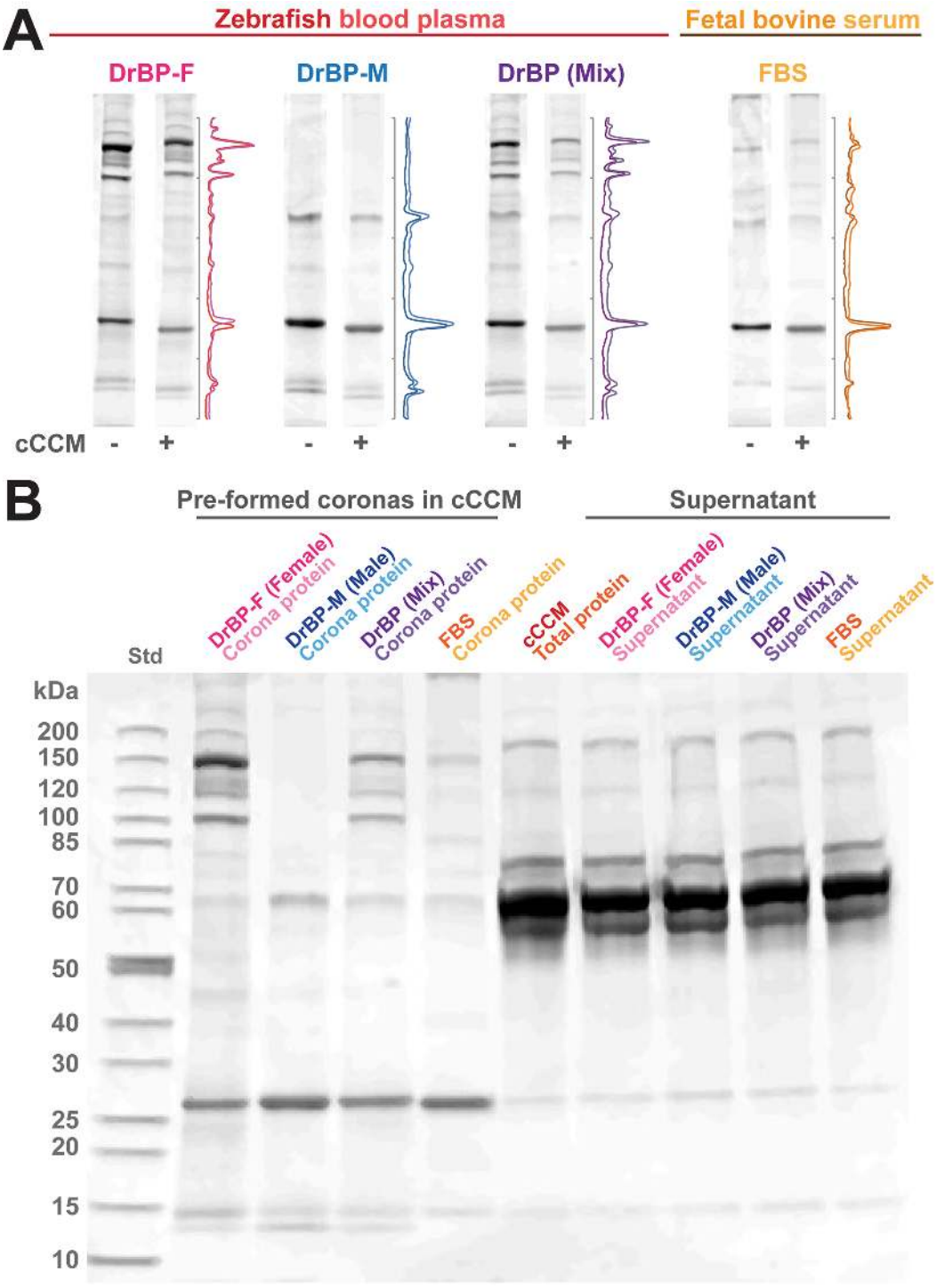


**Figure S5.** Protein corona profiles under the exposure condition (2 h incubation at 26°C in cCCM). (A) Side-by-side comparisons of the protein patterns before (left) and after (right) the 2 h incubation of the $SiO_2$

nanoparticle-protein complexes in cCCM. Note that each set of the two lanes derives from two representative gels. The associated spectra in solid lines are intensity profiles normalized to the molecular weight standard in each gel, allowing direct comparisons of the run length and intensity. Intact gel images can be found in Figure S1 (left lanes) and the panel B of this figure. (B) The intact image of the gel, some lanes of which appeared in (A). The remaining lanes show the profiles of free proteins in the supernatant. A representative gel of three independent experiments is shown.

## FITC intensity distribution profile (Fig. S6)

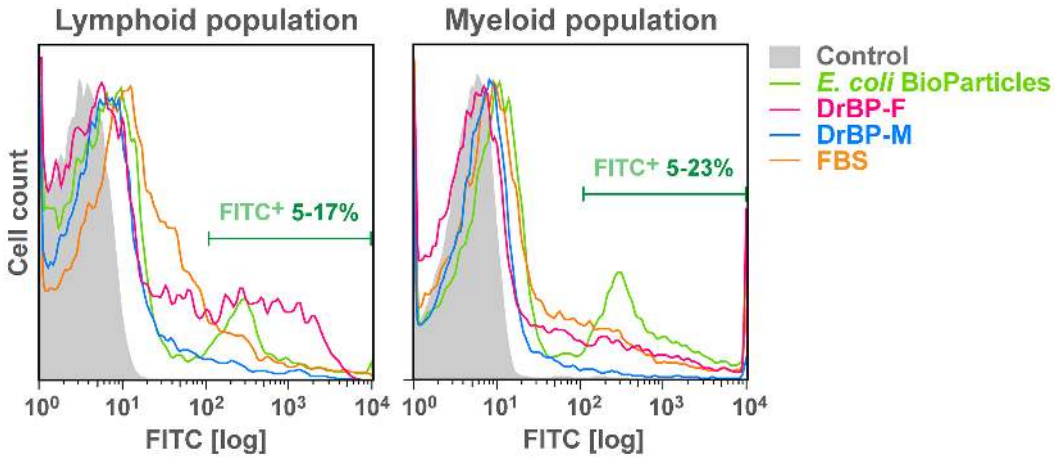


**Figure S6.** Representative profiles of the FITC fluorescence intensity distribution analysed by flow cytometry. Filled histograms and solid lines represent the control and the treatments (50 $\mu$g/ml), respectively. The increases of the cell count in the right tail of the peaks indicate that, during the 2 h exposure, only a minor fraction of the WKM cells accumulated BioParticles or $SiO_2$ nanoparticle-protein complexes to a remarkable extent. Some cells in the myeloid population, in particular in the DrBP-F treatment, had fluorescence intensity higher than the upper threshold; those cell counts were stacked at the end of the tail at the arbitrary fluorescence unit of $10^4$.

**Cellular accumulation of $SiO_2$ nanoparticles, non-pooled (Fig. S7)**

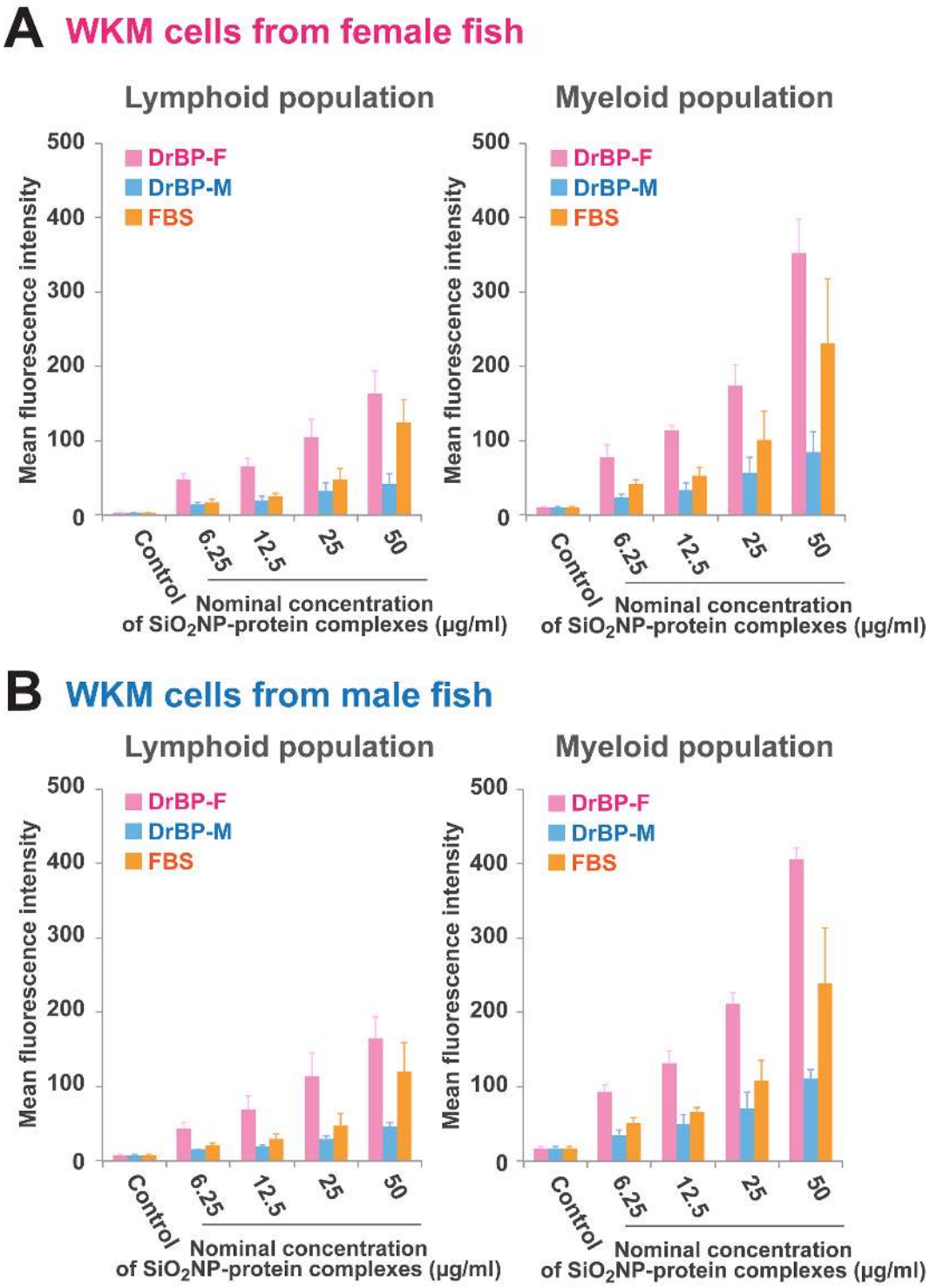


**Figure S7.** Cellular accumulation of $SiO_2$ nanoparticle-protein complexes pre-formed with three

different protein corona types (a non-pooled version of Figure 4). Results for WKM cells harvested from (A) female fish and (B) male fish are shown. Values are mean ± SE of three independent assays. No significant effect of the interaction of sex and the treatments (at 50 $\mu$g/ml) was observed for both of lymphoid and myeloid populations (Two-way ANOVA, $p = 0.795$ for lymphoid and $p = 0.870$ for myeloid).

## References


1. F. Babaei, R. Ramalingam, A. Tavendale, Y. Liang, L. S. K. Yan, P. Ajuh, S. H. Cheng and Y. W. Lam, *J. Proteome Res.*, 2013, **12**, 1580-1590.

2. S. Lindman, I. Lynch, E. Thulin, H. Nilsson, K. A. Dawson and S. Linse, *Nano Lett.*, 2007, **7**, 914-920.

3. M. P. Monopoli, A. S. Pitek, I. Lynch and K. A. Dawson, in *Nanomaterial Interfaces in Biology*, eds. P. Bergese and K. Hamad-Schifferli, Humana Press, 2013, vol. 1025, ch. 11, pp. 137-155.

4. Y. Hayashi, T. Miclaus, C. Scavenius, K. Kwiatkowska, A. Sobota, P. Engelmann, J. J. Scott-Fordsmand, J. J. Enghild and D. S. Sutherland, *Environ. Sci. Technol.*, 2013, **47**, 14367-14375.

5. J. Schindelin, I. Arganda-Carreras, E. Frise, V. Kaynig, M. Longair, T. Pietzsch, S. Preibisch, C. Rueden, S. Saalfeld, B. Schmid, J.-Y. Tinevez, D. J. White, V. Hartenstein, K. Eliceiri, P. Tomancak and A. Cardona, *Nat. Methods*, 2012, **9**, 676-682.

6. C. A. Schneider, W. S. Rasband and K. W. Eliceiri, *Nat. Methods*, 2012, **9**, 671-675.

7. R. N. Finn, *Biol. Reprod.*, 2007, **76**, 926-935.

**Table S1. List of *Danio rerio* blood plasma proteins identified in the hard corona around 70 nm $SiO_2$ nanoparticles.**

**Protein source: DrBP-F (*Danio rerio* blood plasma, female)**

| band ID | Mw range (kDa) | gene/Protein name | accession # | Mw[a] (kDa) | pI[a] | GRAVY score[a] | Mascot score | |
|---|---|---|---|---|---|---|---|---|
| | | | | | | | corona protein | total protein |
| **F1 (tp)** | 120 – 150 | vitellogenin 1 | Q1LWN2 | 149 | 8.74 | 0.019 | 3530 | 7338 |
| | | vitellogenin 4 | F1Q7L0 | 149 | 8.92 | -0.009 | 3429 | 6247 |
| | | vitellogenin 6 | F1QV15 | 150 | 8.83 | -0.016 | 3183 | 6332 |
| | | vitellogenin 5 | F1R2S5 | 149 | 8.84 | -0.012 | 2890 | 6257 |
| | | vitellogenin 7 | A3KMS4 | 149 | 8.76 | 0.009 | 2524 | 5258 |
| **F2 (tp)** | 85 – 100 | vitellogenin 1 | Q1LWN2 | 149 | 8.74 | 0.019 | 1025 | 3654 |
| | | vitellogenin 6 | F1QV15 | 150 | 8.83 | -0.016 | 867 | 3067 |
| | | vitellogenin 4 | E9QFD8 | 149 | 8.86 | 0.014 | 813 | 3048 |
| | | vitellogenin 5 | F1R2S5 | 149 | 8.84 | -0.012 | 787 | 2741 |
| | | vitellogenin 7 | A3KMS4 | 149 | 8.76 | 0.009 | 658 | 1943 |
| | | vitellogenin 2 | Q1MTC4 | 180 | 8.70 | -0.060 | 435 | 1618 |
| **F3 (tp)** | 60 – 70 | vitellogenin 1 | Q90YN8 | 150 | 8.68 | 0.029 | 347 | 1371 |
| | | alpha-2-HS-glycoprotein 1 (fetuin) | Q5U3D8 | 51 | 7.13 | -1.116 | 220 | - |
| **F4 (tp)** | 25 – 30 | apolipoprotein A-I b | E7FES0 | 30 | 6.04 | -0.647 | 2636 | 3384 |
| | | apolipoprotein A-I a | O42363 | 30 | 5.06 | -0.615 | 1915 | 3427 |
| | | vitellogenin 1 | Q1LWN2 | 149 | 8.74 | 0.019 | 706 | 506 |
| **F5 (tp)** | 12 – 15 | Haemoglobin subunit beta-2 | Q90485 | 16 | 7.70 | 0.056 | 844 | 1161 |
| | | Haemoglobin subunit beta-1 | Q90486 | 16 | 7.70 | 0.048 | 815 | 1110 |
| | | apolipoprotein A-II | B3DFP9 | 16 | 6.59 | 0.070 | 803 | 722 |
| | | Novel protein similar to zebrafish haemoglobin alpha-adult 1 | Q6ZM17 | 16 | 8.81 | 0.131 | 569 | - |
| | | novel beta globin* | Q6DGK4 | 16 | 8.92 | 0.046 | 478 | 228 |
| | | haemoglobin, alpha adult 1 | Q803Z5 | 16 | 7.97 | 0.170 | 464 | 1074 |
| | | haemoglobin, alpha adult 2 | Q7SZV9 | 16 | 8.81 | 0.148 | 458 | 1001 |
| | | vitellogenin 5 | F1R2S5 | 149 | 8.84 | -0.012 | 328 | - |
| | | haemoglobin subunit alpha* | Q5BJC7 | 15 | 9.16 | 0.172 | 327 | 336 |
| | | vitellogenin 1 | Q1LWN2 | 149 | 8.74 | 0.019 | 322 | - |
| | | apolipoprotein A-I b | E7FES0 | 30 | 6.04 | -0.647 | 218 | - |

**Protein source: DrBP-M (*Danio rerio* blood plasma, male)**

| band ID | Mw range (kDa) | gene/Protein name | accession # | Mw[a] (kDa) | pI[a] | GRAVY score[a] | Mascot score | |
|---|---|---|---|---|---|---|---|---|
| | | | | | | | corona protein | total protein |
| **M1** | 60 – 70 | alpha-2-HS-glycoprotein 1 (fetuin) | Q5U3D8 | 51 | 7.13 | -1.116 | 753 | - |
| | | alpha-2-HS-glycoprotein 1 (fetuin) | E7FF41 | 51 | 7.01 | -1.131 | 509 | - |
| | | Haemoglobin subunit beta-2 | Q90485 | 16 | 7.70 | 0.056 | 333 | - |
| **M2 (tp)** | 25 – 30 | apolipoprotein A-I b | E7FES0 | 30 | 6.04 | -0.647 | 5157 | 4518 |
| | | apolipoprotein A-I a | O42363 | 30 | 5.06 | -0.615 | 2161 | 3556 |
| **M3 (tp)** | 12 – 15 | apolipoprotein A-II | B3DFP9 | 16 | 6.59 | 0.070 | 1052 | 1708 |
| | | Haemoglobin subunit beta-2 | Q90485 | 16 | 7.70 | 0.056 | 617 | 1956 |
| | | Haemoglobin subunit alpha | Q90487 | 16 | 7.97 | 0.172 | 491 | 1326 |
| | | haemoglobin, alpha adult 2 | Q7SZV9 | 16 | 8.81 | 0.148 | 392 | 1486 |
| | | novel beta globin* | Q6DGK4 | 16 | 8.92 | 0.046 | 370 | 494 |
| | | haemoglobin subunit alpha* | Q5BJC7 | 15 | 9.16 | 0.172 | 274 | 785 |
| | | histone h2b* | R4GE02 | 27 | 10.17 | -0.594 | 211 | - |

**Protein source: FBS (Fetal bovine serum)**

| band ID | Mw range (kDa) | gene/Protein name | accession # | Mw[a] (kDa) | pI[a] | GRAVY score[a] | Mascot score | |
|---|---|---|---|---|---|---|---|---|
| | | | | | | | corona protein | total protein |
| **B1** | 120 – 150 | Thrombospondin-1 | F1N3A1 | 130 | 4.72 | -0.717 | 844 | n.a. |
| | | Complement factor H | Q28085 | 140 | 6.43 | -0.651 | 473 | n.a. |
| **B2** | 60 – 70 | Serum albumin | B0JYQ0 | 69 | 5.95 | -0.432 | 1499 | n.a. |
| | | Serum albumin | P02769 | 69 | 5.82 | -0.429 | 1414 | n.a. |
| | | Complement component 3 | A0A0F6QNP7 | 187 | 6.46 | -0.349 | 948 | n.a. |
| | | Alpha-1-antiproteinase | P34955 | 46 | 6.05 | -0.056 | 766 | n.a. |
| | | Apolipoprotein A-I | P15497 | 30 | 5.71 | -0.619 | 547 | n.a. |
| **B3** | 25 – 30 | Apolipoprotein A-I | P15497 | 30 | 5.71 | -0.619 | 5450 | n.a. |

GRAVY, Grand average of hydropathy.
* Annotated based on the BLAST (blastp) hits.
[a] Before post-translational modification, computed using SIB Bioinformatics Resource Portal (ExPASy) from the complete amino acid sequence.

**Table S2. List of *Danio rerio* blood plasma proteins identified in the protein source but not in the hard corona.**

**Protein source: DrBP- F (*Danio rerio* blood plasma, female)**

| band ID | Mw range (kDa) | gene/Protein name | accession # | Mw[a] (kDa) | pI[a] | GRAVY score[a] | Mascot score | |
|---|---|---|---|---|---|---|---|---|
| | | | | | | | corona protein | total protein |
| **F2tp** | 85 – 100 | alpha 2-macroglobulin* | F1QQY9 | 128 | 5.36 | -0.097 | - | 1610 |
| | | alpha 2-macroglobulin* | X1WC44 | 125 | 5.28 | -0.100 | - | 1567 |
| | | alpha 2-macroglobulin-like* | F1R8N2 | 160 | 5.38 | -0.063 | - | 1466 |
| | | alpha 2-macroglobulin-like | A0JMP8 | 160 | 5.30 | -0.068 | - | 1423 |
| | | alpha 2-macroglobulin-like* | X1WBT0 | 160 | 5.94 | -0.130 | - | 1179 |
| **F3tp** | 60 – 70 | Serotransferrin | F1R858 | 74 | 6.61 | -0.344 | - | 4635 |
| | | complement component c3a, duplicate 2 | F1QV29 | 185 | 6.42 | -0.333 | - | 1944 |
| | | complement component c3a, duplicate 1 | B8JKW4 | 183 | 6.17 | -0.320 | - | 1657 |
| | | vitellogenin 5 | F1R2S5 | 149 | 8.84 | -0.012 | - | 1229 |
| | | complement component c3a, duplicate 3 | Q3MU73 | 185 | 6.48 | -0.312 | - | 1076 |
| | | complement component c3a, duplicate 3 | F1QX13 | 185 | 6.49 | -0.322 | - | 970 |
| | | complement component 5 | F1R0S4 | 118 | 7.95 | -0.177 | - | 967 |
| | | vitellogenin 7 | A3KMS4 | 149 | 8.76 | 0.009 | - | 934 |
| **F4tp** | 25 – 30 | apolipoprotein A-IV b, tandem duplicate 1 | F1QHR0 | 30 | 4.77 | -0.625 | - | 1859 |
| | | apolipoprotein A-IV b, tandem duplicate 2 | B3DHC5 | 29 | 4.78 | -0.630 | - | 1732 |
| | | apolipoprotein A-IV b, tandem duplicate 3 | F1QJD1 | 29 | 4.76 | -0.589 | - | 1526 |
| **F5tp** | 10 – 15 | Actin, cytoplasmic 1 | Q7ZVI7 | 42 | 5.30 | -0.213 | - | 1024 |
| | | actin, alpha 1a, skeletal muscle | F1QUN8 | 42 | 5.22 | -0.227 | | 690 |
| | | Histone H4 | Q0D294 | 11 | 11.36 | -0.574 | - | 289 |

**Protein source: DrBP- M (*Danio rerio* blood plasma, male)**

| band ID | Mw range (kDa) | gene/Protein name | accession # | Mw[a] (kDa) | pI[a] | GRAVY score[a] | Mascot score | |
|---|---|---|---|---|---|---|---|---|
| | | | | | | | corona protein | total protein |
| **M1tp1** | 60 – 70 | Serotransferrin | F1R858 | 74 | 6.61 | -0.344 | - | 4973 |
| | | complement component c3a, duplicate 2 | F1QV29 | 185 | 6.42 | -0.333 | - | 2492 |
| | | complement component c3a, duplicate 1 | B8JKW4 | 183 | 6.17 | -0.320 | - | 1838 |
| | | complement component c3a, duplicate 3 | Q3MU73 | 185 | 6.48 | -0.312 | - | 1540 |
| | | Carboxylic ester hydrolase | F1R9X5 | 60 | 5.49 | -0.056 | - | 1289 |
| | | Carboxylic ester hydrolase | Q1LYL6 | 61 | 5.43 | -0.041 | - | 1076 |
| | | complement component 5 | F1R0S4 | 118 | 7.95 | -0.177 | - | 1037 |
| **M1tp2** | 60 – 70 | Hemopexin | Q6PHG2 | 51 | 6.14 | -0.522 | - | 4245 |
| | | Serpin peptidase inhibitor, clade A, member 7 | Q5XJ64 | 43 | 5.16 | -0.340 | - | 1489 |
| | | Fibrinogen, B beta polypeptide | Q6NYE1 | 54 | 8.07 | -0.679 | - | 1101 |
| | | apoliporotein Ba | E7FBD3 | 496 | 5.44 | -0.216 | - | 1062 |
| | | serpin peptidase inhibitor, clade A, member 7 | A8E5C1 | 43 | 5.16 | -0.351 | - | 933 |
| **M2tp** | 25 – 30 | apolipoprotein A-IV b, tandem duplicate 1 | F1QHR0 | 30 | 4.77 | -0.625 | - | 1888 |
| | | apolipoprotein A-IV b, tandem duplicate 2 | B3DHC5 | 29 | 4.78 | -0.630 | - | 1696 |
| | | apolipoprotein A-IV b, tandem duplicate 3 | F1QJD1 | 29 | 4.76 | -0.589 | - | 1515 |
| **M3tp** | 10 – 15 | Haemoglobin subunit beta-1 | Q90486 | 16 | 7.70 | 0.048 | - | 1905 |
| | | Myoglobin | Q6VN46 | 16 | 6.96 | 0.086 | - | 387 |

GRAVY, Grand average of hydropathy.
***** Annotated based on the BLAST (blastp) hits.
[a] Before post-translational modification, computed using SIB Bioinformatics Resource Portal (ExPASy) from the complete amino acid sequence.